CHALMERS
UNIVERSITY OF TECHNOLOGY

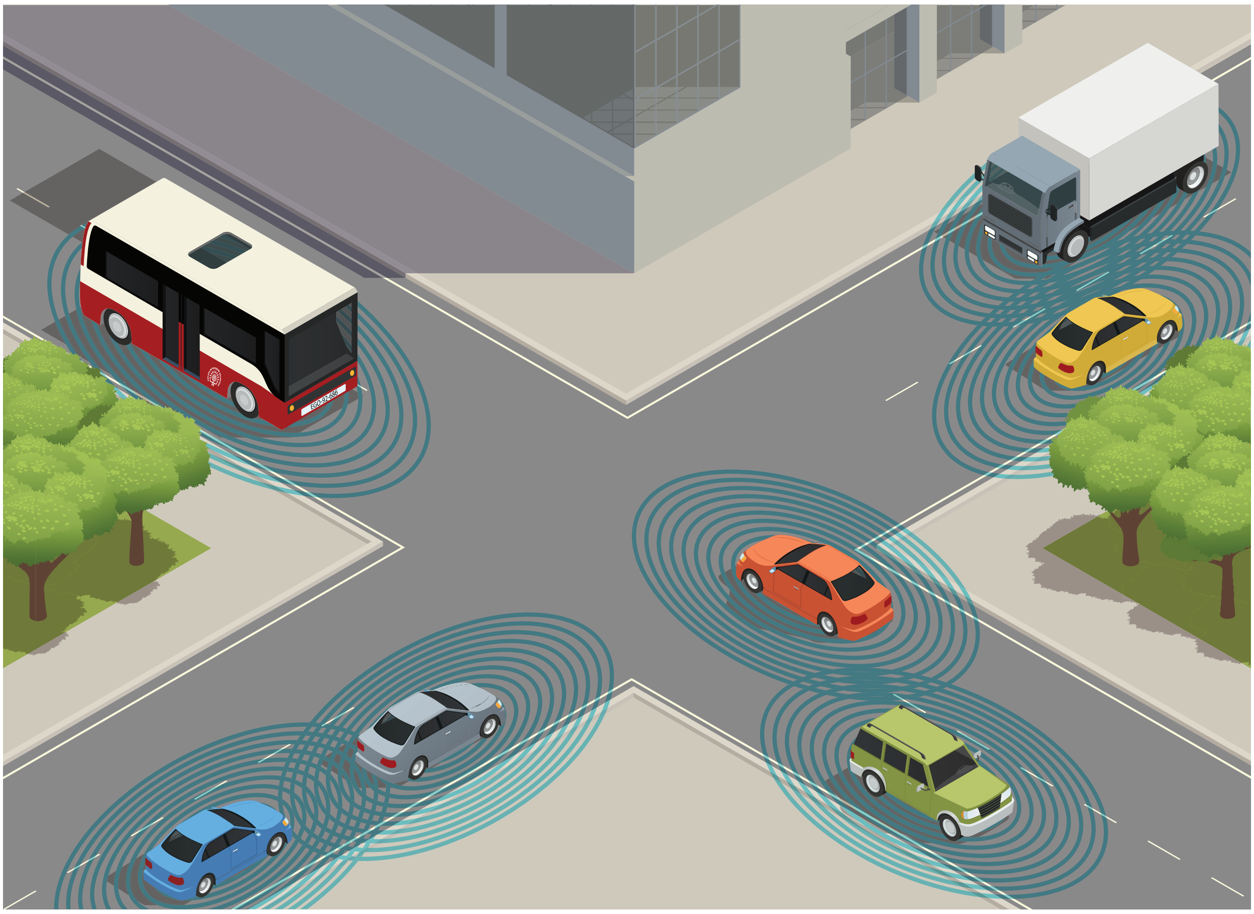

FMCW-Based Automotive Radar Communications for Intersection and Real-Traffic Scenarios

Master's thesis in Communication Engineering

MUSTAFA METE

Department of Electrical Engineering
CHALMERS UNIVERSITY OF TECHNOLOGY
Gothenburg, Sweden 2020

Master's thesis 2020:NN

FMCW - Based Automotive Radar Communications for Intersection and Real-Traffic Scenarios

MUSTAFA METE

Department of Electrical Engineering
Division of Communication Engineering
Chalmers University of Technology
Gothenburg, Sweden 2020

FMCW-Based Automotive Radar Communications for Intersection and Real-Traffic Scenarios
MUSTAFA METE

Supervisor: Canan Aydogdu, Department of Electrical Engineering
Examiner: Henk Wymeersch, Department of Electrical Engineering

Master's Thesis 2020:NN
Department of Electrical Engineering
Communication and Antenna Systems
Chalmers University of Technology
SE-412 96 Gothenburg
Telephone +46 31 772 1000
Email:metem@student.chalmers.se; eem.mustafamete@gmail.com

Front Cover: Illustration of vehicles with RadCom units crossing an intersection.

(From [1]. Adapted with permission.)

Typeset by the author using LaTeX
Printed by Chalmers Reproservice
Gothenburg, Sweden 2020

FMCW-Based Automotive Radar Communications for Intersection and Real-Traffic Scenarios
MUSTAFA METE
Department of Electrical Engineering
Chalmers University of Technology

Abstract

Although it comprises a small part of the road, millions of traffic accidents occur at an intersection every year. This rate is expected to decrease by technological advancements in autonomous driving since automotive radars provide drivers local awareness. In order to get an accurate detection, increasing automotive radars deployed on a vehicle seems like the most promising solution. However, it is challenging to coordinate the allocation of available time and frequency resources among present automotive radars, which leads to an increase in mutual interference among radars, and a decrease in the performance of automotive radars.

This thesis project aimed at proposing a joint radar communication system protocol (RadCom) as a solution to mitigate mutual interference mentioned above by enhancing the existing work on RadCom and implementing it on complex traffic scenarios. Proposed RadCom protocol was evaluated by using different traffic scenarios consisting of four-way intersections with straight, right-left- turn traffic and straight traffic based on real-time data. The evaluation results were represented by comparing the simulated performance of RadCom by using different metrics.

The results from the evaluation demonstrated that we achieved enhancing radar communications by coordinating multiple Frequency Modulated Continuous Wave (FMCW) radars placed on different parts of a vehicle with the radars placed on other vehicles in complex traffic scenarios. Moreover, the proposed RadCom managed in broadcasting a communication packet in acceptable delays.

Keywords: Intersection, VANET, RadCom, joint radar communication, automative radars, CSMA, FMCW, mutual interference, collision avoidance, vulnerable period.

Acknowledgements

This thesis project has been such a journey that I have learned so much, not only about my profession and the academic world but also about myself.

First and foremost, I would like to express my appreciation to my supervisor Ph.D. Canan Aydogdu for her consistent guidance throughout the process. She helped me to make the right decision and has been there whenever I felt stuck. Furthermore, I would like to thank my examiner, Prof. Henk Wymeersch, for his feedback, which was on point and had a direct impact on several steps of the study. Akin Bacioglu, thanks for sparing your time to proofread my thesis and other tips regarding the visuals in the report.

From the bottom of my heart, I would like to say big thank you to my mom Hulya, my dad Selahattin, and my sister Sinem, for standing by me when needed and supporting all my decisions, no matter what the outcome has been. Without you, I couldn't be where I am today.

Lastly, I want to express my gratitude to the founder of the Republic of Turkey, Mustafa Kemal Ataturk, who has been a perfect role model for Turkish people of all ages for decades by glorifying hard work, perseverance, and positive sciences.

MUSTAFA METE, Gothenburg, June 2020

Contents

List of Figures

List of Tables

1 Introduction

In the last decade, the public expectation for ground transportation systems has shown a dramatic increase. Owing to the technological advancements in the Internet, computers, analysis, control, and communication technologies, drivers want their vehicles to support and provide functions such as self-driving and future collision avoidance [4, 5]. Therefore, autonomous driving is attracting more attention, and it undertakes some responsibilities of drivers so that they might devote much more time to other things while driving. However, this interest, together with the increase in the number of vehicles brought along some challenges such as traffic congestion and collision. In order to maximize safety and minimize risks and efficiency during transportation, both academia and industry carry out many projects ranging from cooperative systems where vehicles communicate with each other and their environment, such as signalized traffic [6, 7]. Vehicular communication is one of the promising solutions to these challenges since it provides a vehicle the information of neighboring vehicles [4].

Automotive radars within human-driven vehicles offer various services ranging from park assist to collision warning, which also make them one of the vital players in the automotive industry in terms of safety and efficiency. The advancements in the automotive radars since their first application have made them an integral part of vehicular communication systems. Hence, another notable solution to address the challenges mentioned above is using joint radar communication systems. They are based on using the same hardware and the same radio spectrum for radar and communication systems [4, 8, 9]. Radar communication between vehicles mitigates mutual interference between radar systems, so it has the potential to increase traffic efficiency and road safety.

1.1 Problem Description

According to the research conducted by The Federal Highway Administration (FHA) in USA, roughly 2.5 million traffic accidents occur at an intersection every year, although it comprises a small part of the road [10]. By technological advancements in autonomous driving, this rate is expected to decrease since automotive radars provide a driver the local awareness as detection of neighboring vehicles. In order to get an accurate detection, increasing the amount of automotive radars deployed on a vehicle seems like the most promising solution [11]. However, it is challenging to coordinate the allocation of available time and frequency resources among present automotive radars, which leads to an increase in mutual interference among radars. Mutual interference gives rise to a decrease in the performance of radar [12].

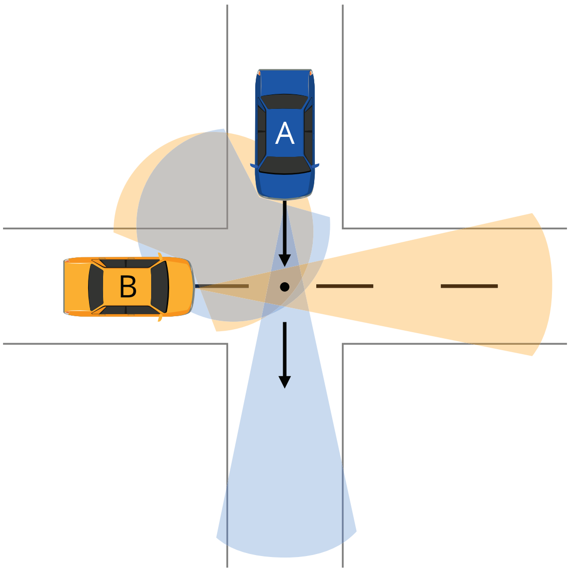

Figure 1.1: Mutual interference of signals from two cars with front and corner radars approaching an intersection.

To exemplify mutual interference, Figure 1.1 shows a traffic scenario where two vehicles with identical FMCW radars approach an intersection from different lanes. They are starting their transmission simultaneously, and radar signals are exposed to interference. Since the receiver detects only received signal which comprises of back-scattering signal and interfering signals, it is highly probable that the output of signal processing steps to resolve the targets result in the wrong detection.

In order to overcome such mutual interference, one particular method that stands out is RadCom, which is based on using the same hardware and the same radio spectrum for radar and communication systems [4, 8, 9]. However, previous studies related to RadCom [12, 9], only deal with simple traffic scenarios such as a single-hop scenario where all radars see other radars or multihop scenarios with one or two fleets and exclude complex traffic scenarios including an intersection. Therefore, this study has three objectives:

- Enhancing the RadCom protocol proposed by [12] so that it can coordinate multiple FMCW radars placed on different parts of a vehicle with the radars on other vehicles running in complex traffic scenarios,
- Identifying which types of the FMCW radar were needed and how they would be deployed,
- Evaluating the performance of the improved RadCom protocol in complex traffic scenarios including four-way intersection and real-time driving scenarios by using different performance metrics.

This thesis mainly concerns a RadCom protocol for traffic scenarios including non-signalized intersections and real-time traffic data with the position traces of vehicles, and investigates that how RadCom units can be coordinated by cross-layer radar data.

In order to simplify our design, we assume that

- the number of radars on a vehicle is six so that the Field of View (FOV) of these radars could form a complete region around the vehicle,
- the dimensions of a Volvo XC90 [13] is used for vehicles' layout,
- radar and communication signals only propagate through a LOS path in case one exists, applying a geometry-based deterministic vehicular channel model by ignoring reflections from the environment (ground, buildings) or other vehicles,
- the most critical source of link blockage is vehicles [44], so we omit the possible blockage sources except for vehicles and consider only LOS paths between vehicles,
- vehicles approaching the intersection decelerate, pass the intersection at the same speed and accelerate again after passing the intersection, so we ignore vehicular kinematics such as overtaking,
- distributed, non-signalized four-way intersections with straight, right-left- turn traffic are used on simulated traffic flow, thereby no traffic lights or central coordination unit exists,
- and real-time driving scenarios are based on the realistic vehicular mobility traces for varying number of vehicles.

Besides, to evaluate the performance of the improved RadCom protocol, our performance metrics are

- the fraction of radar blinds, which is described as the ratio of the number of interfering RadCom units to the total number of RadCom units,
- the data rate per RadCom unit,
- convergence time that is the required time for all RadCom units in a vehicular traffic scenario to overcome and reach acceptable mutual interference,
- the time for each vehicle to converge in a fully connected vehicular network,
- and, the delay time for a vehicle to broadcast the communication packet.

1.2 Related Work

The ultimate goal of an intelligent Transportation System (ITS) is to provide collision-free driving and lighten the driver's mental load. RadCom emerges as a promising solution on the way to reach this goal. Since it is a very new research area for both the industry and academia, there have been different studies, including various techniques on this topic. They all seek the answer "how to make the integration between radar and communication systems more efficient, practical in intelligent transportation". Most studies focus on orthogonal frequency division multiplexing (OFDM) for radar communication because of its advantages, such as showing high performance despite propagation through varying conditions [8, 14]. In [15] detection and estimation algorithm based on kernel least mean square (KLMS) is proposed by using OFDM waveform while [16, 17] estimate detection parameters by using cylix prefixed OFDM (CP-OFDM). In [4], a distributed medium access control (MAC) protocol based on OFDM is developed to accomplish the spectrum allocation for radar and communication systems. The disadvantage of OFDM systems is intercarrier interference (ICI) caused by the intrapulse Doppler effect [18]. That's why [19] suggests a receiving model including the intrapulse and intersubcarrier Doppler effects. In this approach, a joint radar-range communication system, and Doppler estimation is accomplished by using the maximum likelihood (ML) method. Even though it shows better performance compared to the others, some complexity problems still exist when there are multiple targets. There are also many ongoing RadCom based on OFDM oriented research studies [20] to increase system performance.

There are other waveforms and channel methods that support Radcom. For instance, [21] uses the IEEE 802.11ad waveform to predict detection parameters through autocorrelation while [8] uses Cyclic prefixed single carrier (CP-SC) waveform to design a detection and estimation algorithm. [14] proposes a dual-functional radar communication (DFRC) technique for predicting vehicle motion parameters while [22] suggests a joint access channel method to mitigate interference.

To support the development of RadCom, some of the existing studies focus on software or hardware design of radar systems. In [23] a software-defined radar (SDR) system is designed, and it enables real-time radar imaging. In [12, 9] an approach based on the FMCW waveform is proposed and the small part of radar bandwidth is allocated for communication system. Besides, they create a virtual traffic scenario, including identical long-range FMCW radars deployed on the windshields and rear window. Then, the transmission time is scheduled for facing radars positioned on different vehicles. Their simulation results show that interference among radar signals is considerably reduced without sacrificing detection performance from an accuracy viewpoint.

1.3 Contributions

This thesis extends the studies [12, 9] by the incorporation of more complex traffic scenarios, such as an intersection or real traffic. We have enhanced the RadCom protocol proposed by [12, 9] to support the coordination of multiple FMCW radars placed on the same vehicle with the radars on other vehicles by identifying which types of the FMCW radar were needed and how they would be deployed.

To evaluate the performance of the improved RadCom protocol, we designed virtual driving scenarios that include a distributed, non-signalized intersection with multiple vehicles by considering cooperative intersection management methods. These scenarios enabled an increase in the number of vehicles and acquired different vehicular typologies in which vehicles are randomly or equally distributed among the lanes.

1.4 Thesis Outline

The organization of the thesis is as follows. Following the introduction, Chapter 2 provides an overview of essential background on intersection management methodology, FMCW radar basics, vehicle to vehicle communication, Joint Radar Communication (RadCom) systems and the application of FMCW Radars on Rad-Com. Chapter 3 explains the details of how a distributed, non-signalized intersection is designed, FMCW radars' deployment and identification, a wireless propagation channel by identifying radar and communication links is determined to implement the enhanced RadCom protocol. Chapter 4 describes the stages of development of the present RadCom protocol provided by [12, 9]. In Chapter 5, the simulation results obtained by changing the input parameters are discussed to evaluate the performance of RadCom under the varying conditions followed by the conclusion.

2
Background Theory

This chapter provides the theoretical background on intersection management, basic information related to FMCW radars, vehicular communication, and RadCom with the applications of FMCW on it.

2.1 Intersection Management

Autonomous driving technology requires intersection management in terms of traffic capacity, safety, and collision avoidance, although it comprises the small part of the road. An intersection is a shared zone that vehicles demand to use simultaneously, so it needs to be organized and scheduled. A lot of different studies have been carried out to manage intersection in the research and development of intelligent transportation. Based on completed and ongoing studies, intersection management can be investigated under three subheadings as below [2]:

2.1.1 Intersection Modelling

Since we need to consider the performance of our proposed RadCom protocol in complex traffic scenarios firstly, we need to identify the most common intersection geometry that can be classified under three categories as below:

2.1.1.1 Space and Time Discretization

The intersection is a shared resource, so the passing order of vehicles can be considered a discretized resource allocation and optimization problem. Where discretized time slots and spaces are assigned to vehicles that will enter an intersection. Space discretization can be done in different ways depending on intersection shape, as shown in Figure 2.1.

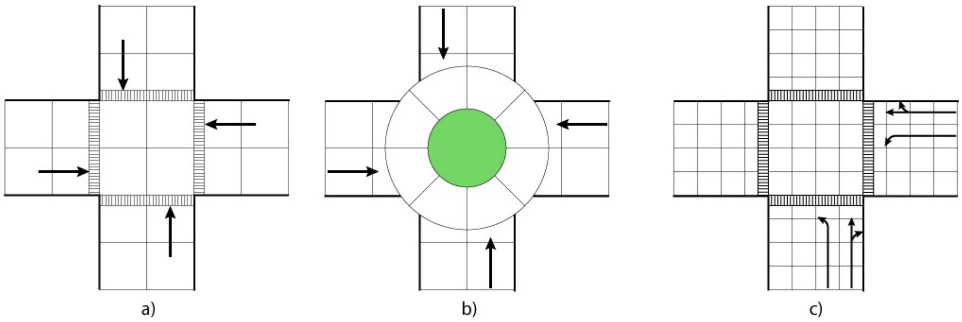

Figure 2.1: Illustration of intersection discretization: a) four-way intersection with straight, b) roundabout, c) four-way intersection with straight, right-turn and left-turn traffic. (Source: Modified from [2])

2.1.1.2 Trajectory Modelling

Intersection is assumed as a well-organized place and vehicles coming up intersection follow the predefined routes to pass intersection without regarding traffic lights, control units, etc as shown in Figure 2.2.

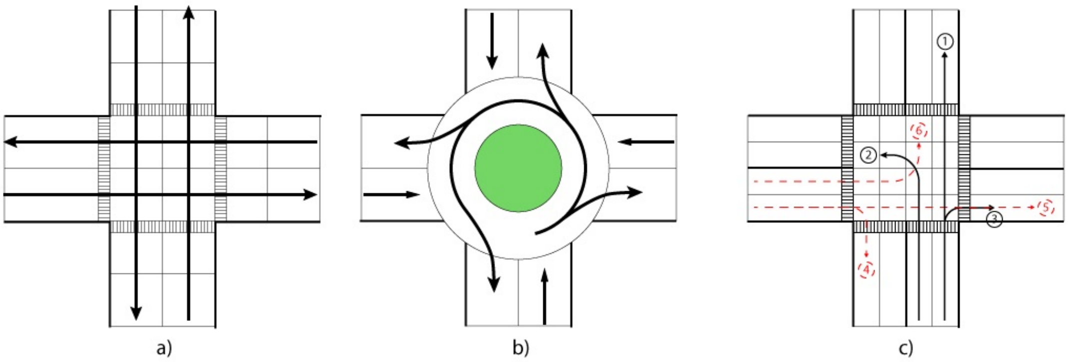

Figure 2.2: Trajectory Illustration: a) four-way intersection with straight, b) roundabout, c) four-way intersection with straight, right-turn and left-turn traffic. (Source: modified from [2])

The aim of trajectory modelling is to minimize the collision risk and maximize the efficiency of intersection usage, etc. by identifying safe travel routes for vehicles. In order to enhance these metrics, vehicle control parameters like velocity, acceleration, braking and throttle, etc., can be taken into account. The constrains on the modelling thereby can be identified. Based on each vehicle's trajectory, it can be determined which vehicle has a potential of colliding with another one in the course of passing the intersection. The trajectory with no risk of collision is classified as safe pattern and the vehicle which has it utilize the intersection safely. As shown in the Figure 2.2(c) some trajectories such as 1 and 4 build a safe pattern while 2 and 6 do not. Trajectory modelling has a wide usage are such as in a traffic flow analysis systems [24], and for collision avoidance on winding roads [25].

2.1.1.3 Collision Region Modelling

Assuming that the vehicles entering the intersection follow the predefined routes, probable collision regions can be established by the help of the two methods mentioned above, as shown in Figure 2.3. The complexity in the implementation of previous two other methods is considerably reduced, as stated in [6], where collision-free path planning was done by using the combination of integrated scheduling and path planning.

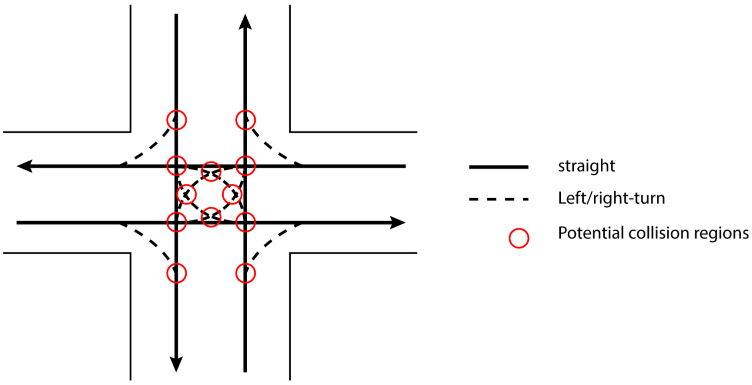

Figure 2.3: Illustration of potential collision regions on a four way intersection. (Source: modified from [2])

2.1.2 Cooperative Intersection Management (CIM)

In order to enhance traffic safety and efficiency in Intelligent Transportation, vehicles and infrastructures are unified by using cooperative vehicular techniques. It can be used to solve the intersection passing by cooperative communication in vehicular networks, which is called Cooperative Intersection Management (CIM). Where all vehicles collaborate with each other, so the passing and traffic on the intersection is scheduled and coordinated depending on the collected knowledge from cooperative environment. There are two types of communication in cooperative systems which are vehicle-to-vehicle (V2V) and vehicle-to-infrastructure (V2I), respectively [26]. CIM can be classified as centralized or distributed depending on whether there is a central control unit or not.

2.1.2.1 Centralized CIM

Centralized CIM includes a coordination unit that is responsible for collecting and broadcasting knowledge from the environment to vehicles, as shown in Figure 2.4. Furthermore, a decision is centrally taken by the coordination unit. According to the broadcast, a vehicle can decide how and when to pass the intersection safely.

2.1.2.2 Distributed CIM

Distributed CIM has no central control units, and vehicles create a communication network through Vehicular ad-hoc network (VANET) [27], as shown in Figure 2.5.

In a distributed CIM, decisions are taken locally based on knowledge of the environment, and then vehicles agree on passing the intersection to minimize the collision risk. Different methods are combined with CIM, such as in [28], cooperative vehicular network system with the different types of vehicles was exhibited as centralized and distributed with the possibilities of Cognitive Radio.

Since this thesis focused on radar communication between vehicles forming a VANET, we utilized distributed CIM in our study.

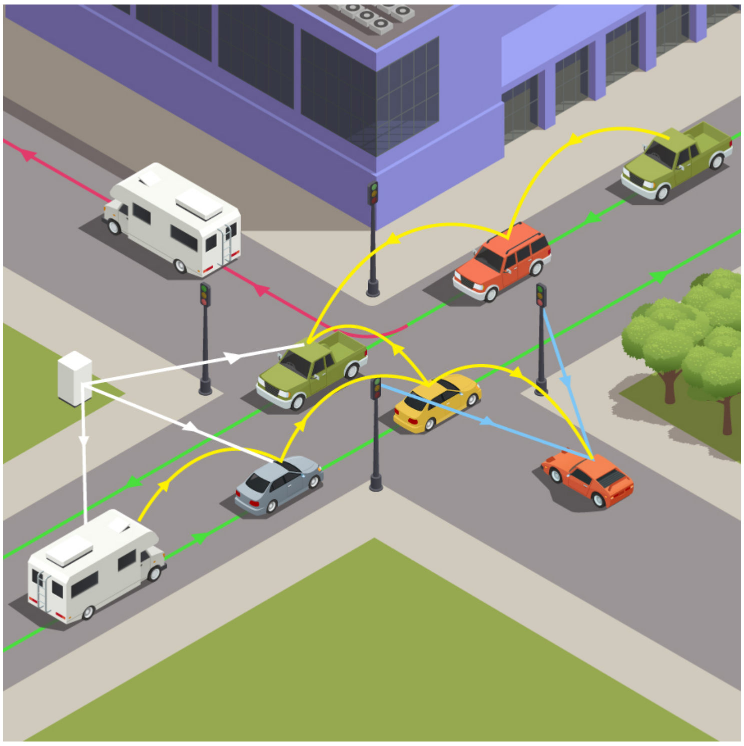

Figure 2.4: Illustration of centralized CIM. Central control unit manages intersection passing.(From [1]. Adapted with permission.)

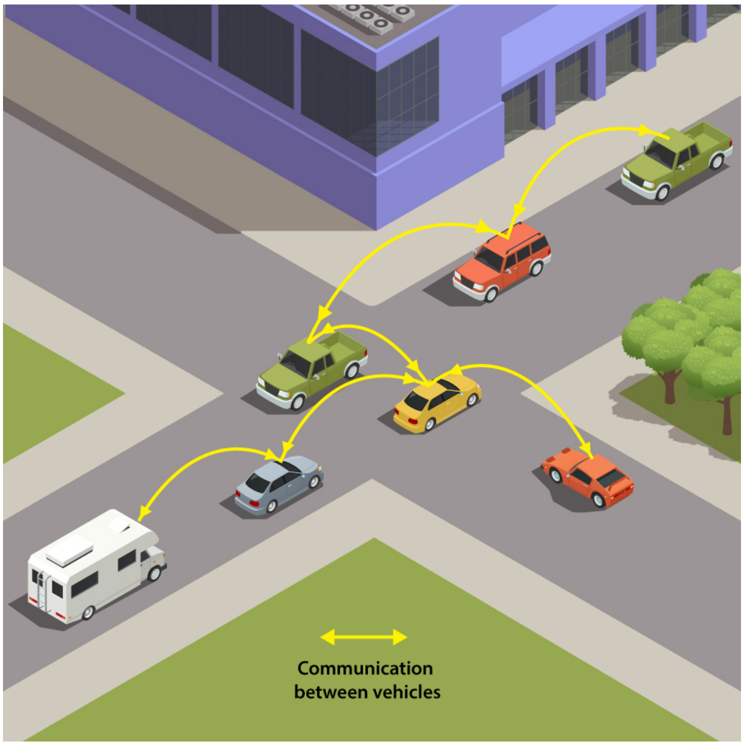

Figure 2.5: Illustration of distributed CIM. Vehicles make CIM decisions through VANET.(From [1]. Adapted with permission.)

2.1.3 Traffic Coordination

Depending on the existence of traffic lights or traffic controllers, traffic flow on the intersection can be coordinated in two ways, which are signalized intersection and non- signalized intersection.

2.1.3.1 Signalized Intersection

At a signalized intersection, traffic lights are used to coordinate the traffic flow, as shown in Figure 2.6, and it is a critical component in terms of traffic congestion and collision. Today signalized intersection management is enhanced by combining different technical methods such as in [7]; an integrated waiting area was proposed with the signalized intersection where all lanes were assumed as variables and circularly assigned to different directions on the intersection keeping the traffic flow the same. They achieved a decrease in delay and an increase in traffic efficiency at the intersection. Another study [29] combined shock wave analysis and Bayesian Network to predict some traffic variables such as congestion and journey time etc. at a signalized intersection, and the simulation results showed an encouraging prediction rate.

2.1.3.2 Non-Signalized Intersection

Contrary to signalized, Non-signalized intersection does not have any traffic controllers like a traffic light or sign, etc. as shown in figure 2.7. Intersection passing is

Figure 2.6: Illustration of signalized intersection with traffic lights.(From [1]. Adapted with permission.)

managed through eye contact among drivers. It may result in unwanted situations like traffic accidents, so non-signalized intersection has been evolving with promising technological progress involving cooperative communication like V2V and V2I, collision avoiding system and connected vehicles, etc. In [30], a cooperative driving algorithm for connected and automated vehicles was designed by using model predictive control. According to simulation results, the developed algorithm enhanced safety, traffic efficiency at the intersection.

In order to make the virtual traffic scenario more complex, a non signalized intersection is a more appropriate way to coordinate traffic flow in our study.

Figure 2.7: Illustration of non-signalized intersection (From [1]. Adapted with permission.)

2.2 Radar Basics

Radar is the abridgment of Radio Detection and Ranging System, which uses electromagnetic waves to acquire the location and distance of an object. It performs by transmitting signal to and receiving the reflected signal from the target object. Depending on the application, it operates in the different frequency ranges of the radio spectrum, such as the mm (millimeter) band of 30–300GHz for automotive, navigation, high-resolution image processing etc., [31, 11]. Radars can be classified as primary and secondary depending on whether there is a transponder on the target. In a primary radar, the antenna transmits a radar pulse to and receives a small portion of signal reflected back from target and then calculates the range by using the time delay between transmitted and reflected signals. Current automotive radars however, in a secondary radar, a longer yet reliable range can be accomplished since more powerful signal is reflected to a transmitter through a transponder compared to primary radars [32].

There are several more kinds of radar configuration depending on the application area and technology in use such as bistatic radar, continuous-wave (CW) radar, and pulse-Doppler radar[31] For example, in CW radar systems, a continuous wave signal with the same frequency is transmitted, and it is not possible to acquire range information since time delay measurement cannot be achieved. However, it can measure the relative speed of the target by Doppler shift of the receiving signal, which is a difference in the frequency caused by the movement of one of the transmitters, the target, or both. It is often preferred in traffic control and military applications. In pulsed radar systems, the good range resolution is achieved by repeating short and powerful pulses. It performs well in resolving the targets located far away. It requires high power to keep the signal to noise ratio (SNR) at an acceptable level. In basic radar systems, the range (R) is calculated by using the round-trip time that transmitted signal takes to and from the target during propagation, and it can be expressed given formula.

$$R = \frac{c\Delta t}{2} \tag{2.1}$$

where Δt is the round-trip time in [s] and c is the speed of light in meters per second.

FMCW is one of the most common types of automotive radars for short-range since it provides fine range and relative velocity estimation with high accuracy in terms of cost and efficiency. It transmits frequency modulated continuous ramp signals generated by a voltage-controlled oscillator (VCO) [31, 33]. FMCW radar systems support many modulation methods or waveforms based on measurement purposes. Popular modulation methods are:

- Stepped waveform (Staircase voltage): It transmits consecutive trains of sinusoidal signals at different frequencies to targets. By clarifying a convenient value as step frequency, unambiguous measured range is set to maximum.
- Triangular waveform: A beat frequency is obtained because of target range and Doppler frequency. The components of beat frequency are combined as difference from rising and falling edge of signal. The radial velocity and the target range can be determined by using these components. The disadvantage for triangle waveform is the ghost detection that is caused by resultant Doppler frequencies in the existence of a number of reflections.
- Square-wave form (simple frequency-shift keying,FSK): This modulation type provides an exact distance determination for a short range by making the comparison of the phases obtained from two reflected signals' frequencies. Drawback of this modulation is that it is not possible to distinguish multiple targets since reflected signals from different targets in the radar range are not distinguishable from each other.
- Sawtooth waveform: It supports the detection in large range and the Doppler shift on range estimation can be omitted.

In order to realize the proposed RadCom in our study, FMCW radars based on sawtooth waveform are used as automotive radars that are mounted on vehicles because of their detection performance for long and short range. Also, they have the potential to detect very small movements. It transmits a modulated sinusoid signals [34] that is called chirps whose frequency increases linearly over time as depicted in Figure 2.8.

There are several performance metrics to evaluate a detection system. These metrics for an automotive radar are velocity resolution, range resolution, direction estimation, maximum measurable range and maximum measurable velocity [11, 35]. These

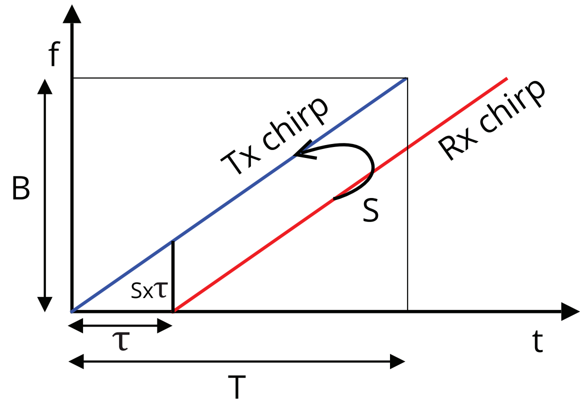

Figure 2.8: Illustration of chirp signal, with frequency as a function of time.

rely on technical properties of the chosen radar such as carrier frequency, sampling frequency, chirp duration T and bandwidth B as shown in figure 2.8. In a FMCW radar, sampling rate F_s of analog-to-digital converter (ADC) and the slope of the modulated chirp signal constraint the ability to detect the maximum range.

The round-trip (τ_{trip})time states the length of time between transmitted and received chirps [34] and for the chirp shown in figure 2.8, it is expressed as

$$\tau_{trip} = \frac{2d}{c} \tag{2.2}$$

where d is distance from the radar to the target.
In addition, maximum measurable range (d_{max}) [34] is given by

$$d_{max} = \frac{cf_s}{2S} \tag{2.3}$$

where S is the slope of chirp signal and it is defined as the ratio of the chirp bandwidth to the chirp duration and is given by

$$S = \frac{B}{T} \tag{2.4}$$

The range resolution is essential to automotive radars and it expresses the ability to resolve two closely positioned targets by considering the minimum distance required between them [11, 35]. The resolution (ΔR) relies only on the ramp chirp bandwidth B so bigger bandwidth enables to have a better resolution. It can be expressed as

$$\Delta R = \frac{c}{2B} \tag{2.5}$$

Another notable performance metric on automotive radars is velocity resolution (Δv) (2.6) that the capability to resolve moving targets' velocities with high accuracy [11, 34]. As expressed in the equation the longer frame time transmitter in FMCW radar has, the better velocity resolution is can be obtained on the receiver side.

$$\Delta v = \frac{\lambda}{2T_f} \tag{2.6}$$

where T_f is frame duration that is the sum of chirps' duration and processing time and λ represents the wavelength of carrier signal. There are some constraints such as the carrier frequency and chirp duration for a radar to resolve the radial velocities unambiguously. The maximum measurable relative velocity states that the maximum, unambiguously detected velocity (v_{max}) and it is given by

$$v_{max} = \frac{\lambda}{4T} \tag{2.7}$$

As the equations above suggests, chirp bandwidth and chirp duration are crucial in selection or design of a radar. For instance, better range resolution and maximum measurable range require larger bandwidth. Consequently, we need to consider the trade-off between these two parameters and radar performance metrics when designing a radar system [11, 34, 35].

2.3 V2V Communication Basics

Vehicular communication is getting notable attention from the point of road safety and traffic efficiency by critical technological advancements in research and industry area. Taking a more in-depth look at the last two decades, we saw firstly in the US that 5,9 GHz bandwidth was dedicated to communication between V2V and then followed by Vehicle to Everything (V2X) [21]. This frequency band also is named Dedicated Short-Range Communication (DSRC), and it has been allocated to communication channels in tens of megahertz bandwidth [4]. Meanwhile, the European Telecommunication Standards Institute (ETSI) has defined intelligent transportation system (ITS)-G5 standards [5]. Both DSRC and (ITS)-G5 standards are built on the IEEE 802.11p technology, and the maximum data rate is at around 27 Mbps [21]. Vehicular communication based on either one of both standards has allowed vehicles to broadcast their attributes to their neighbors, as shown in figure 2.9. However, in a crowded and dynamically changing topology, both can have difficulties such as packet collision, link blockage caused by another vehicle, and communication-to-communication interference, etc. since medium accesses control (MAC) layer in IEEE 802.11p is used for wireless local area networks (WLAN) with low mobility [36]. Vehicular communication can be considered as a real-time system, and the essential part of this system is MAC [36, 37].

VANET is designed by a wireless network of vehicles to overcome aforementioned difficulties. VANET is created by the communication among distributed vehicles and there is no central control unit for coordination and sharing resources. That's why, the allocation of a centralized MAC protocol for a distributed and dynamically changing topology requires much effort [38].

The IEEE 802.11p MAC protocol with Carrier Sense Multiple Access (CSMA) algorithm and the exponential back-off enables to listen channel activity [38]. In this

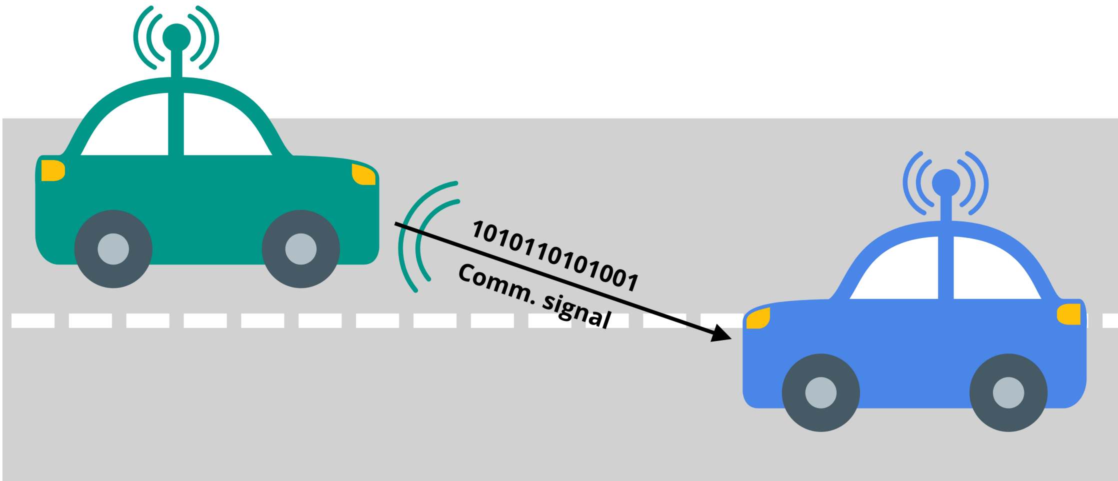

Figure 2.9: Illustration of vehicular communication between two vehicles.

procedure [38, 12], a vehicle which intends to broadcast its communication packet needs to listen to the channel for some time and then, if the channel is sensed free, it can broadcast the packet. However, if the channel is sensed busy, the vehicle has a random back-off value that obtained by an exponential distribution and this value is getting decreased while listening to the channel. The vehicle continues to listen to the channel until it gets free again.

2.4 Radar Communications (RadCom)

Radar systems are one of the most prevalent methods to acquire the location information of an object. Studies relevant to the specific radar waveform design result in the enhanced accuracy in the detection and estimation tasks of the object velocity and range. Thereby, FMCW based automotive radars have been most popular in terms of driving safety and local awareness in the automotive industry. Despite the fact that those radars occupy the 77-81 GHz millimeter wave band which is dedicated to 79 GHz, the detection accuracy in automotive radars is not in the aimed levels [4, 22].

Vehicular Communication is another popular method from the point of view of road safety and traffic efficiency. 5.9 GHz band has been dedicated to short range communication that starting between V2V and going on with V2X [4, 8]. However, the rapid increase in user demands from, and advancements on vehicular communication has triggered the scarcity problem in this band spectrum [4, 8, 9].

In recent years, to be able to cope with such challenges, there has been promising research done. One particular study that stands out is called Joint Radar Communication (RadCom), which is based on using the same hardware and the same radio spectrum for radar and communication systems [8, 9]. RadCom not only provides higher efficiency in terms of spectrum and energy consumption but also mitigates mutual interference between radar systems and communication systems

[12, 14]. There are still some difficulties to overcome. If both communication system and radar receiver operate simultaneously, strong self-interference occurs in the radar receiver. The self-interference cancellation between both systems requires full-duplex operation [14].

There are many ongoing RadCom oriented research studies, and they all seek the answer to “how to be able to make the integration between radar and communication systems more efficient, practical in intelligent transportation”. One of them suggests a joint access channel method to mitigate interference [22]. Another one proposed by [39] is using the dual-functional radar communication technique for predicting vehicle motion parameters. The most popular one for RadCom is to use OFDM waveforms because of its advantages, such as showing high performance despite propagation through varying conditions [8, 14].

2.5 The Application of FMCW Radars on RadCom

A RadCom unit, as illustrated in Figure 2.10, is facilitated by making some modifications on radar hardware, and the input to the transmitter is be altered to radar and communication. Similarly, on the receiver side, the antenna is shared by radar and communication modules. Thereby, the transmitter on the RadCom unit can convey either radar signals or communication signals at different times just like the receiver can capture receiving radar signals or communication signals at different times [12, 40].

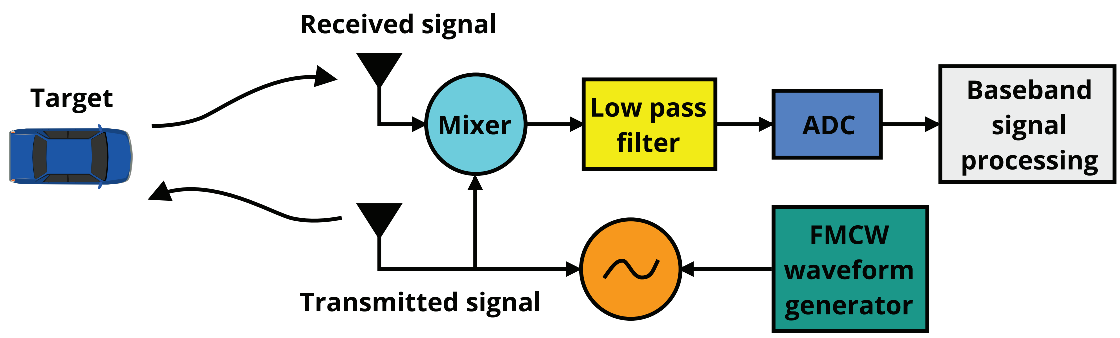

Figure 2.10: Block diagram of a RadCom unit (Source: modified from [3])

A sequence of chirps transmitted by radar, reflections from multiple targets, and the time is required to process received signals are shown in Figure 2.11. Here, T_f is frame time that is the sum of chirps' duration and processing time. The FMCW radar transmits a sequence of chirps which are frequency modulated continuous waves and a chirp can be mathematically expressed by

$$c(t) = \exp(j2\pi(f_c + \frac{B}{T}t)t) \tag{2.8}$$

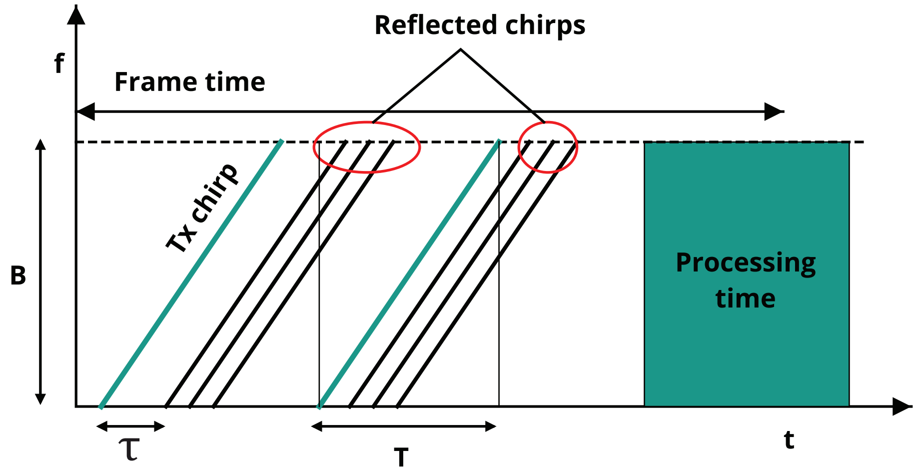

Figure 2.11: Frequency versus time FMCW chirp with reflected chirps from multiple targets

where f_c represents carrier frequency, T is chirp duration, B denotes radar bandwidth, and t is time, and the transmitted signal by an FMCW radar is given by

$$s(t) = \sqrt{P_{\text{tx}}} \sum_{n=1}^{N} c(t - nT) \tag{2.9}$$

where P_{tx} denotes power transmitted by radar, and N represents the total number of chirps transmitted in a time frame.

Since we are in antenna far field region, captured power P_{rx} (2.10) by receiver antenna can be found from free space propagation model [32, 3].

$$P_{rx} = \frac{P_{tx} G_{\text{tx}} G_{\text{rx}} \lambda^2 d^{-2}}{(4\pi)^2} \tag{2.10}$$

where G_{tx} and G_{rx} are gains for transmitter and receiver in turn and d denotes the distance between transmitter and receiver. Since we use identical radars, G_{tx} and G_{rx} take the same value in our simulations that is denoted by G_{trx}.

If it is assumed that vehicles have the potential of scattering the radar signal in high power level as depicted in Figure 2.12, then we need to consider the strength of received signal through back scattering.

If the back scattering is located at a distance d from the transmitter, the received signal power is attenuated by d^{-4} since the transmitted signal travels the same distance twice, and it is given by equation 2.11 which shows us that there is a very strong dependence on distance compared to the other variables [32, 40].

$$P_{rx} = \frac{P_{tx} G_{\text{tx}} G_{\text{rx}} \sigma \lambda^2 d^{-4}}{(4\pi)^2} \tag{2.11}$$

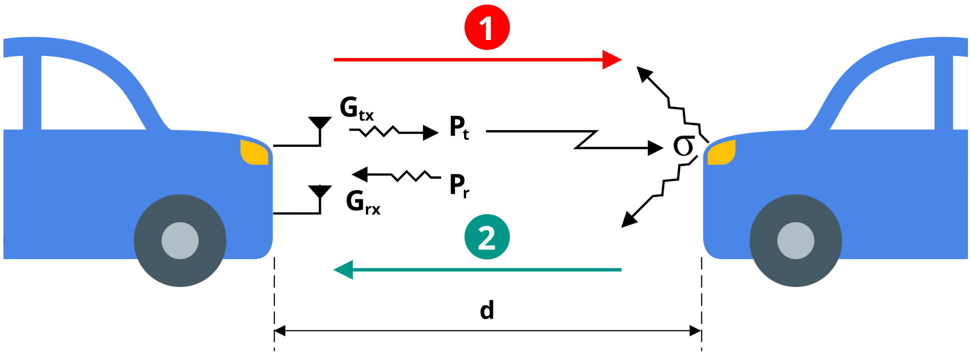

Figure 2.12: Multiple back scattering from a target vehicle towards a receiver

In the given radar equation where σ denotes target cross-section area (RCS) [m^2], and it states the reflectivity of an object in the radar receiver's direction.

At the receiver side first, the received signal is mixed with a copy of transmitted chirp by a mixer. The output signal is called intermediate frequency (IF) signal, which comprises a signal with harmonics. Next, ADC samples the output signal with the sampling rate Ts. The sampled signal is ready to be processed by the digital signal processor (DSP). After signal processing processes on the sampled signal, frequencies will be estimated. A sample n, from the sequence of the received signal sampled by ADC where there is a single scattering target, can be mathematically expressed by [32, 12, 3]

$$r_n = \sqrt{\gamma P_{\text{tx}} d^{-4}} \exp\left(j2\pi \frac{B(2d/c - 2\tau_D)}{T} nT_s \right) + w_n \tag{2.12}$$

In the given equation τ_D represents Doppler time shift, $\tau_D = Tvf_c/Bc$ that caused by a time-varying distance, v is the relative speed, w_n denotes additive white Gaussian noise and is radar cross section for a target, $\gamma = G_{\text{tx}} G_{\text{rx}} \lambda^2/(4\pi)^2$.

In the presence of K targets that are located at different distances, the received signal is the superposition of K backscattered signals. The equation is rewritten for n^{th} sample as below, and it is also assumed that there is the only line of sights (LOS) between target and radar [35, 12].

$$r_n = \sum_{i=1}^{K} \sqrt{\gamma P_{\text{tx}} d_i^{-4}} \exp\left(j2\pi \frac{B(2d_i/c - 2\tau_{\text{Di}})}{T} nT_s \right) + w_n \tag{2.13}$$

2.5.1 Mutual Interference Analysis and Modelling

In order to understand the behavior of a radar when it is interfered, an interference model that covers the mutual interference caused by multiple targets is introduced. Let us consider a traffic scenario where identical FMCW radars deployed on two vehicles that are approaching the intersection on the opposite lanes. Besides, vehicle A is assumed to have an ego radar while assuming vehicle B to have an interfering radar. The distance between two radars is d, and τ is the relative time delay, which states how long after interfering radar starts transmission following the ego vehicle's starting transmission. Arrival time of interfering signal in the receiver of ego radar is $\tau + d/c - \tau_D$ as shown in Figure 2.13.

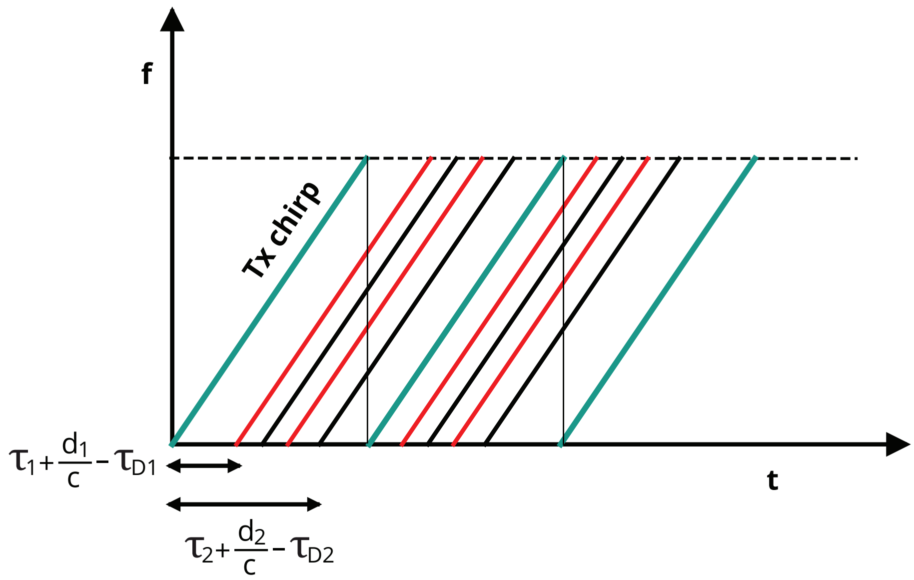

Figure 2.13: Back scattering signals and mutual interference of signals from others around. Green colored chirps represent transmitted, black ones are back scattering and red ones represent interfering signals.

A sample $\tilde{r}_n$ that is taken from the sequence of the received signal sampled by ADC can be expressed in Equation 2.14 two ways depending on the relation between τ and vulnerable period V_{per} [12].

$$\tilde{r}_n = \begin{cases} r_n & \tau \notin V_{per} \\ r_n + \sqrt{\gamma P_{\mathrm{tx}} d^{-2}} \exp\left(j2\pi \frac{B(\tau + d/c - \tau_D)}{T} nT_s\right) & \tau \in V_{per} \end{cases} \tag{2.14}$$

The vulnerable period is defined as the set of τ values in which the ego radar is interfered by another. When τ is not within V_{per}, the received signal is not exposed to interference, and for this reason, it is expressed by 2.12. However, if τ is within V_{per} it received signal is exposed to interference, and it takes the signal form expressed in Equation 2.14. In the presence of K targets that are located at different distances, the received signal is the superposition of the back scattered signals and interfering signals. Equation is rewritten for n^{th} sample as below

$$\tilde{r}_n = r_n + \sum_{\tau_i \in V_{per}} \sqrt{\gamma P_{\mathrm{tx}} {d_i}^{-2}} \exp\left(j2\pi \frac{B(\tau_i + d_i/c - \tau_{\mathrm{Di}})}{T} nT_s\right) \tag{2.15}$$

If the radars, which can cause interference, perform at out of V_{per}, the received signal is not exposed to interference and, for this reason, expressed by Equation 2.13.

Otherwise, it has a total of back scattering and interfering signals.

As understood from Equations (2.14, 2.15), an interfering signal has a factor by d^{-2} and it has very strong impact on the back scattering signal. Hence, an interfering signal causes performance loss in detecting systems such as mis-detection or ghost target detection.

3

System Modelling

This chapter introduces the technology being used in designing traffic scenarios based on complex virtual traffic and real-time traffic data, selecting and placing automotive radars, identifying vehicular LOS paths, and selecting wireless propagation channel.

3.1 Distributed, Non-Signalized Intersection Design

The design and coordination methods explained in Chapter 2 comprised a basis for our distributed, non-signalized intersection design that was used on simulated traffic flow, thereby no traffic lights or central coordination unit existed. We defined a cooperative schedule algorithm based on trajectory and collision region modeling where vehicles follow predefined routes [41]. First, all the possible routes that a vehicle follows while approaching, passing and leaving an intersection were described by considering traffic rules. Then, potential collision regions and safe trajectories were established depending on vehicles' directions. A safe trajectory here represents a route being collision free. Next, it was assumed that vehicles with safe trajectories were scheduled to pass the intersection at one and the same time.To visualize this, let's consider a four-way intersection with straight, left-turn and right-turn as depicted in Figure 3.1 and assume that vehicle A moves on lane 3 and vehicle B moves on lane 7.

According to this assumption only four collision free driving scenarios exists, and vehicles can pass intersection at the same time,

1. Vehicle A moves from lane 3 to lane 4, while vehicle B moves from lane 7 to lane 8.
2. Vehicle A moves from lane 3 to lane 6, while vehicle B moves from lane 7 to lane 8.
3. Vehicle A moves from lane 3 to lane 4, while vehicle B moves from lane 7 to lane 2.
4. Vehicle A moves from lane 3 to lane 6, while vehicle B moves from lane 7 to lane 2.

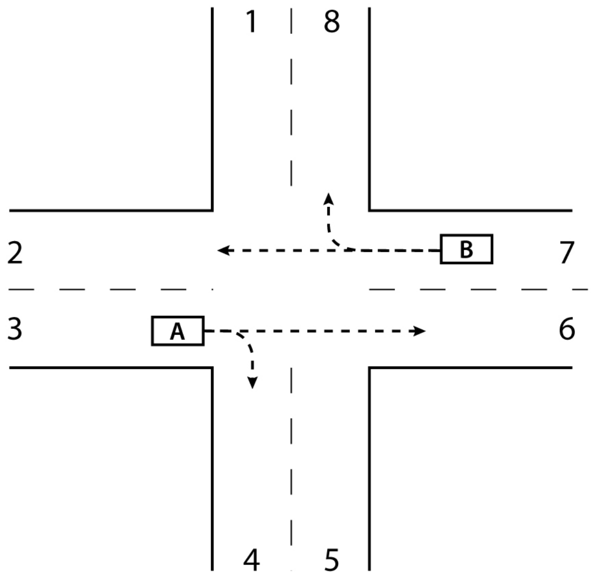

Figure 3.1: Illustration of four-way intersection with safe trajectories.

A collision is the one of inevitable facts of traffic and it may usually occur as depicted in figure 3.2, when

- two vehicles move along the same lane (A, B),
- two vehicles from different lanes pass the same junction area simultaneously (A, C).

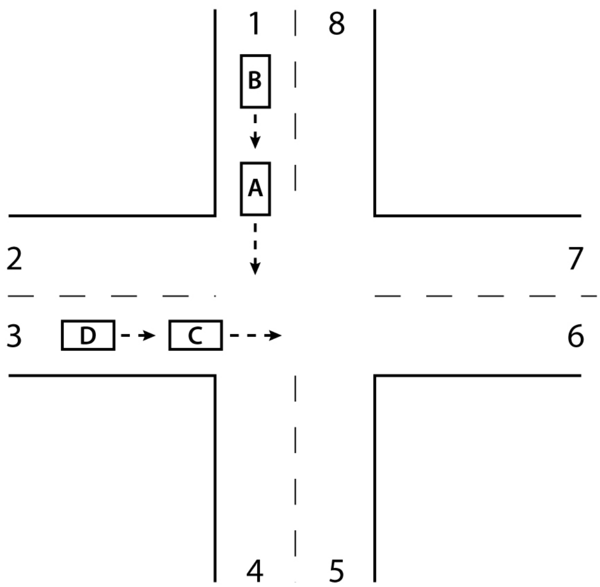

Figure 3.2: Illustration of four-way intersection with collision risk.

In order to guarantee healthy traffic flow, we need to minimize the collision risk. Minimizing was achieved as shown in Figure 3.3 by

1. identifying trajectory profile of each vehicle one by one,
2. defining initial position of a vehicle according to previous one's trajectory,
3. calculating approximate time difference (t) when previous vehicle enters and leaves the intersection and then converting this time into distance ($t.v$),
4. calculating next vehicle's initial position (x_b), by adding the calculated distance together with safety gap between two consecutive vehicles into the previous one's initial position (x_a).

As a result of minimizing, non-safe trajectories were converted into the safe ones.

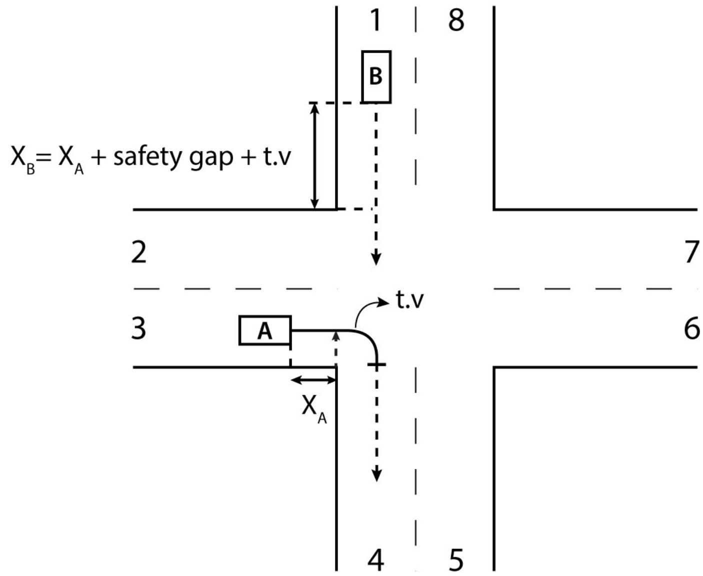

Figure 3.3: Illustration of minimizing process's application.

Where,

- x_A: The initial position of Vehicle A (m)
- x_B: Computed initial position for Vehicle B (m)
- t: Travel time of Vehicle A to pass the intersection

We finally have designed a driving scenario including a distributed, non-signalized intersection with multiple vehicles and it was simulated by Matlab's (R2019-A) Autonomous Driving Scenario Toolbox functions [42]. As shown in Figure 3.4, our design enabled us to increase the number of vehicles and acquire different topologies in which vehicles are randomly or equally distributed among the lanes depending on scenario choice. In Scenario -I, vehicles randomly are distributed among lanes while in Scenario-II, vehicles equally are distributed among lanes. In every run of each scenario, vehicles have different routes since our design algorithms randomly create vehicle trajectories. Besides, vehicles approaching intersection decelerate, pass the intersection at the same speed and accelerate again after passing the intersection.

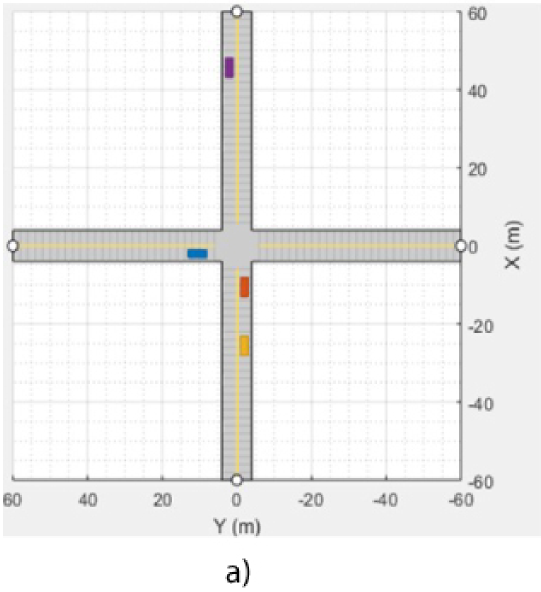

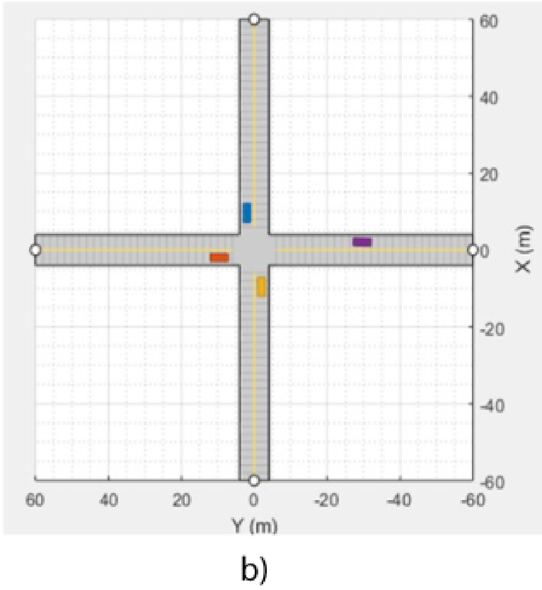

Figure 3.4: Design of distributed, non-signalized intersection. a) four-way intersection with randomly distributed vehicles (Scenario-I) b) four-way intersection with equally distributed vehicles (Scenario-II)

3.2 Radar Deployment on a Vehicle

The most popular vehicular automotive radar type is FMCW radars, and they can be classified according to their range measurement capability and field of view (FOV). They are long-range radar (LRR), medium-range radar (MRR), and short-range radar (SRR) respectively [43]. They have different functional responsibilities, and their common technical properties along with their applications are listed in Table 3.1 [43, 44].

Radar Type	**Long-Range (LRR)**	**Medimum-Range (MRR)**	**Short-Range (SRR)**
Range(m)	$10 - 250$	$1 - 100$	$0.15 - 30$
Azimuth FoV(deg)	±15	±75	±80
Elevation FoV(deg)	±5	±5	±10
Applications	Automotive cruise control	blind-spot detection	obstacle detection

Table 3.1: Classification of Automotive Radars Based on Range Measurement Capability.

To increase the local awareness by automotive radars, we mounted six radars on a vehicle. Of these six radars, two LRR and four MRR were selected by considering their range capabilities and FOVs. LRR was chosen for front and back radars, while MRR was chosen for front and back corner radars. We used the dimensions of a Volvo XC90 [13], assuming that LRR was placed above the windshields and rear window, while MRR placed above the right and left corners of the front and rear bumper as depicted in Figure 3.5. Their technical details were listed in the Table 3.2.

Location	**Front**	**Back**	**Front Right**	**Front Left**	**Back Right**	**Back Left**
Type	(LRR)	(LRR)	(MRR)	(MRR)	(MRR)	(MRR)
Range(m)	$10-200$	$10-200$	$1-80$	$1-80$	$1-80$	$1-80$
Azimuth FOV(deg)	±10	±10	±75	±75	±75	±75
Elevation FOV(deg)	±5	±5	±5	±5	±5	±5
Yaw Angle(deg)	0	-180	-60	60	-120	120

Table 3.2: Technical Details of Automotive Radars Used in Our Design.

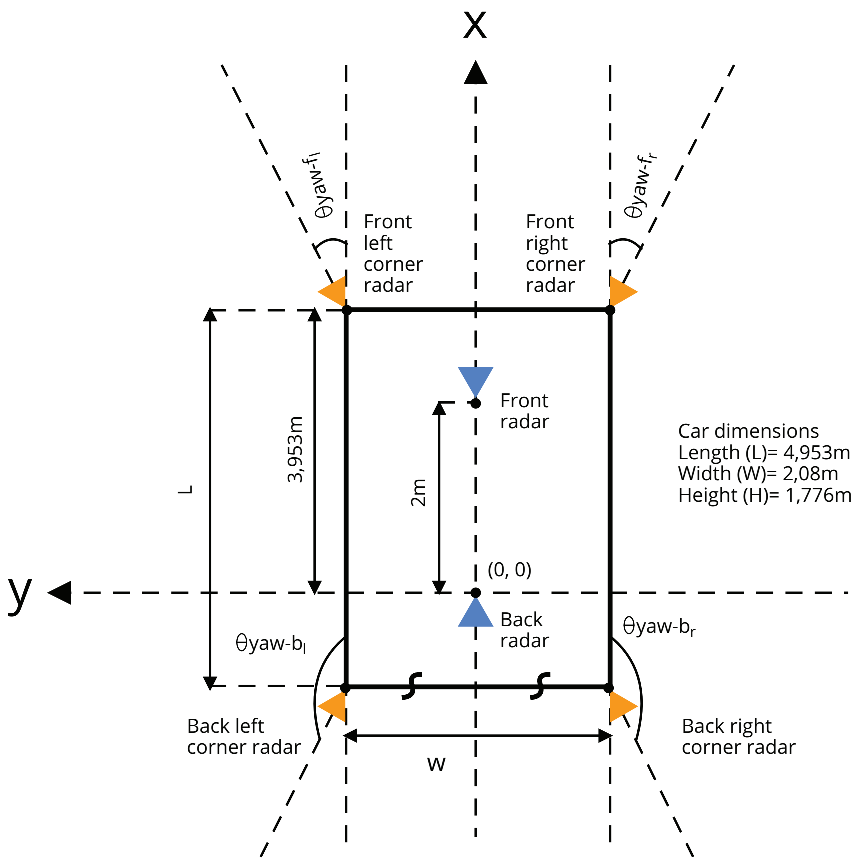

Figure 3.5: Illustration of the radars' placement on a vehicle

The radar placements and the FOV covered were simulated by the Matlab's autonomous driving scenario toolbox functions. By this placement, a circular coverage area was created around the vehicle. In addition, two adjacent automotive radars were assigned different frequency bands in order to avoid adjacent radar interference, whereas the same frequency band was used for opposite radars, since their FOVs did not intercept each other.

Yaw angle represents the instant deviation of a vehicle from a straight route as depicted in the Figure 3.6 and the x-axis denotes the straight route. It takes positive values in the anti-clockwise direction.

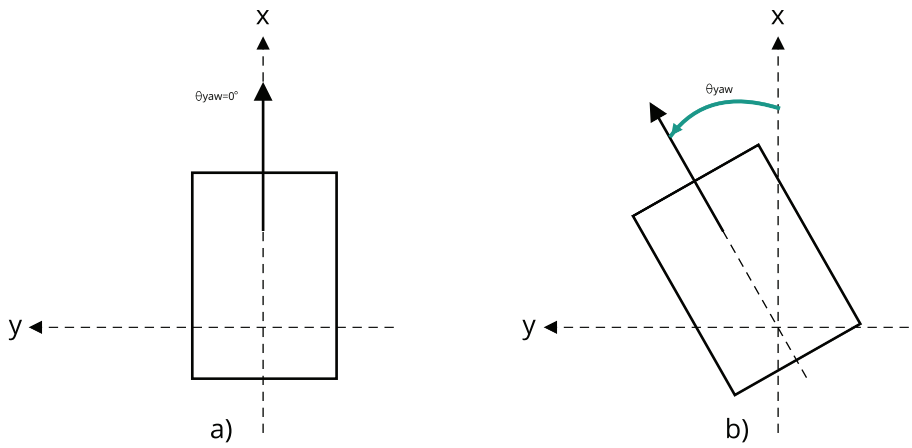

Figure 3.6: Illustration of the yaw angle's variation

3.3 Identifying LOS Paths between Vehicles

In order to identify possible V2V LOS paths that cause interference, we partially used Geometry-Based Propagation Modelling. For this modeling, vehicle locations and the outline of obstacles such as vehicles and buildings are used to distinguish two types of links, which are LOS, non-LOS. According to studies done, one of the most critical sources of link blockage is vehicles [45], so we omit the possible blockage sources except for vehicles and considered only LOS paths between vehicles during our study. The methodology we followed comprises of two basic computational geometry concepts based on the vehicle location information.

3.3.1 The Calculation of Instantaneous Radar's Location

Matlab's Driving scenario tool enables us to read vehicle location information instantaneously. However, it does not provide the information of existing LOS propagation paths. Vehicle information includes a vehicle's position in cartesian coordinates, velocity, and yaw angle, which are:

- x_0: Vehicle's position in x axis on the coordinate plane (m)
- y_0: Vehicle's position in y axis on the coordinate plane (m)
- θ_{yaw}: Vehicle's yaw angle in degrees

Reading x_0 and y_0 correspond to back radar's position information (x_b,y_b), while θ_{yaw} gives front radar's yaw angle θ_{yaw-f} (3.1) and the position information for each radar can be calculated by using these reading values along with geometric equations.

$$\theta_{yaw-f} = \theta_{yaw} \tag{3.1}$$

3.3.1.1 Front Radar

Let us assume that a vehicle is located on the coordinate plane, as depicted in the Figure 3.7. The position information (xf, yf) of the front radar mounted on a vehicle can be calculated by writing some geometric equations from Figure 3.7.

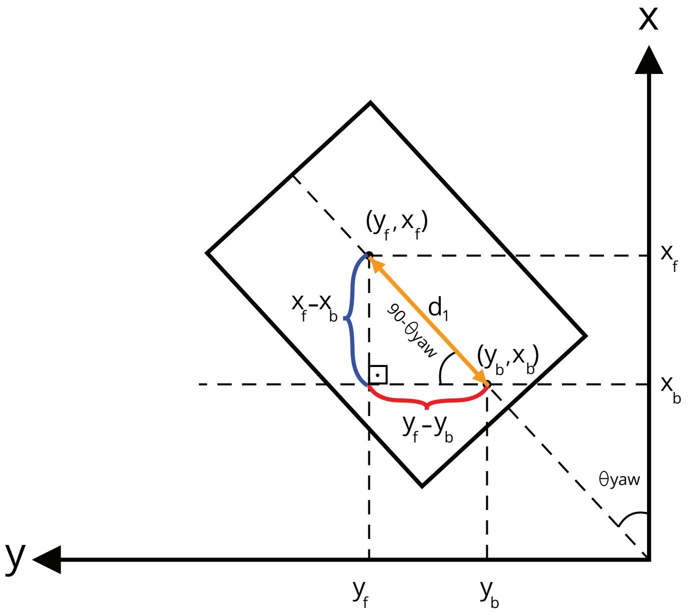

Figure 3.7: Geometric relation between (x_f, y_f) and (x_b, y_b)

$$x_f = d \cdot cos(\theta_{yaw-f}) + x_0 \tag{3.2}$$

Where d is the distance between front and back radars.

$$y_f = d \cdot sin(\theta_{yaw-f}) + y_0 \tag{3.3}$$

3.3.1.2 Back Radar

As aforementioned before, back radar's position information (x_b,y_b) is given by Matlab and yaw angle θ_{yaw-b} can be calculated by Equations given in 3.4 depending on the sign of θ_{yaw}.

$$\theta_{yaw-b} = \begin{cases} \theta_{yaw} + 180 & \text{if } (-180 \leq \theta_{yaw} < 0\ ) \\ \theta_{yaw} - 180 & \text{if } (0 \leq \theta_{yaw} \leq 180\ ) \end{cases} \tag{3.4}$$

3.3.1.3 Front Right Corner Radar

The geometric relation between the front right corner and the back radars can be depicted on the coordinate plane as shown in Figure 3.8. Let's assume that the position information of the front right corner radar mounted on a vehicle to be as (x_{fr},y_{fr}). It can be calculated by using these geometric relations:

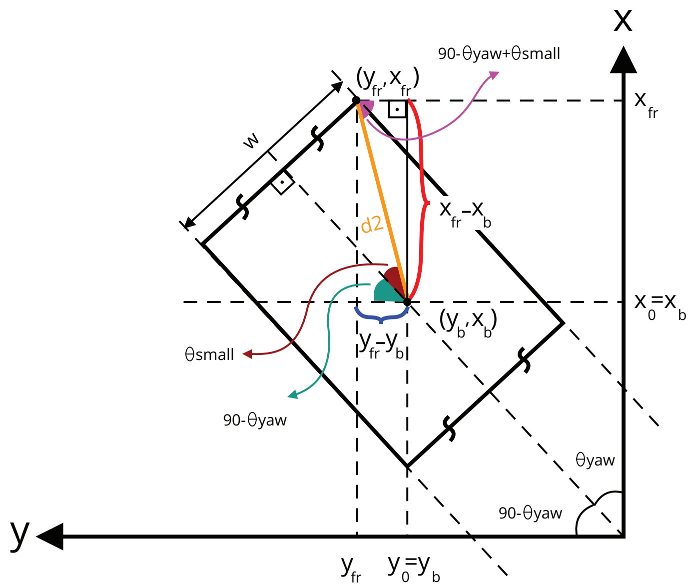

Figure 3.8: Geometric relation between (x_{fr}, y_{fr}) and (x_b, y_b)

$$\theta_{small} = \arcsin \frac{w}{(2 \cdot d_2)} \tag{3.5}$$

$$\theta_{yaw'} = \theta_{small} - \theta_{yawreal} \tag{3.6}$$

$$x_{fr} = d_2 \cdot cos\theta_{yaw'} + x_0 \tag{3.7}$$

$$y_{fr} = d_2 \cdot sin\theta_{yaw'} + y_0 \tag{3.8}$$

where d_2 is the distance between front and front right radars, w is the distance between front right and front left radar pair. Depending on vehicle's direction, a relative yaw angel value θ_{yaw-fr} can be calculated as given in Equation 3.9.

$$\theta_{yaw-fr} = \begin{cases} \theta_{yaw} + 300 & \text{if}(-180 \leq \theta_{yaw} < -120) \\ \theta_{yaw} - 60 & \text{if } (-120 \leq \theta_{yaw} \leq 180\ ) \end{cases} \tag{3.9}$$

3.3.1.4 Front Left Corner Radar

If it is assumed that a vehicles is located on the coordinate plane as depicted in Figure 3.9, the position information (x_{fl},y_{fl}) of the front left radar can be found by using the geometric relation with the position information (x_{fr},y_{fr}) for front right radar.

$$x_{fl} = -w \cdot sin\theta_{yaw} + x_{fr} \tag{3.10}$$

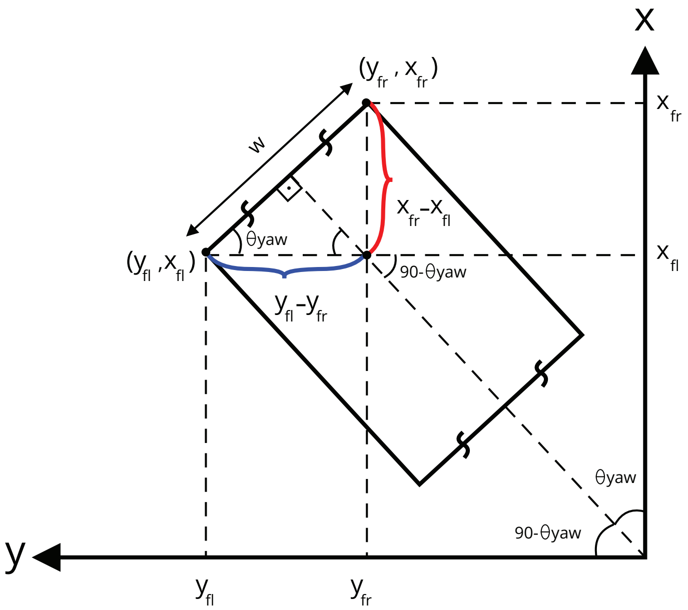

Figure 3.9: Geometric relation between (x_{fr}, y_{fr}) and (x_{fl}, y_{fl})

$$y_{fl} = w \cdot cos\theta_{yaw} + y_{fr} \tag{3.11}$$

Relative yaw angel value θ_{yaw-fl} can be calculated as given in Equation 3.12.

$$\theta_{yaw-fl} = \begin{cases} \theta_{yaw} + 60 & \text{if}(-180 \leq \theta_{yaw} < 120) \\ \theta_{yaw} - 300 & \text{if } (120 \leq \theta_{yaw} \leq 180\ ) \end{cases} \tag{3.12}$$

3.3.1.5 Back Right Corner Radar

The geometric relation between the back right corner and the back radar pair on the vehicle can be illustrated on the coordinate plane as shown in Figure 3.10. If we assume that the position information of back corner radar to be as (x_{br},y_{br}), it can be calculated by following equations.

$$\theta_{small} = \arcsin \frac{w}{(2 \cdot d_3)} \tag{3.13}$$

$$\theta_{yaw\prime} = \theta_{small} + \theta_{yawreal} \tag{3.14}$$

$$x_{br} = -d_3 \cdot cos\theta_{yaw\prime} + x_b \tag{3.15}$$

$$y_{fr} = -d_3 \cdot sin\theta_{yaw\prime} + y_b \tag{3.16}$$

Where d_3 is the distance between back and back right radars. Relative yaw angel value θ_{yaw-br} can be calculated by Equation 3.17.

$$\theta_{yaw-br} = \begin{cases} \theta_{yaw} + 240 & \text{if}(-180 \leq \theta_{yaw} < -60) \\ \theta_{yaw} - 120 & \text{if } (-60 \leq \theta_{yaw} \leq 180\ ) \end{cases} \tag{3.17}$$

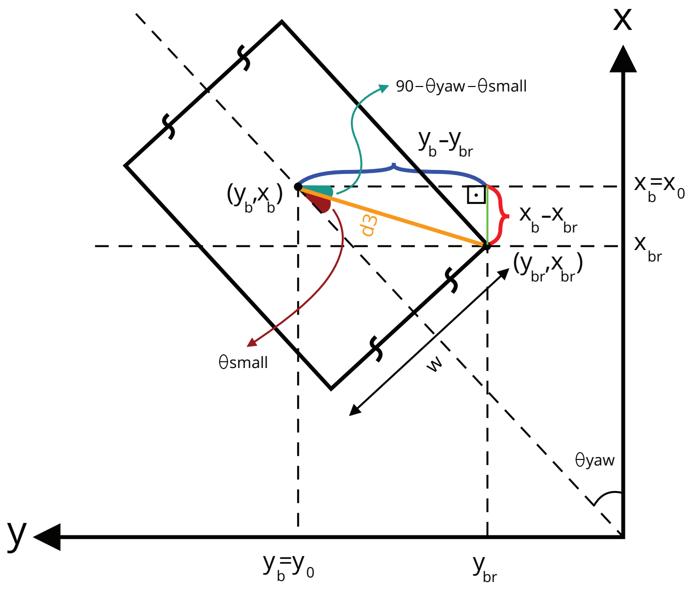

Figure 3.10: Geometric relation between (x_{br}, y_{br}) and (x_b, y_b)

3.3.1.6 Back Left Corner Radar

The position information $(x_{bl}$,$y_{bl})$ of the back left radar can be calculated by using the geometric relation with x_{br},y_{br} shown in Figure 3.11.

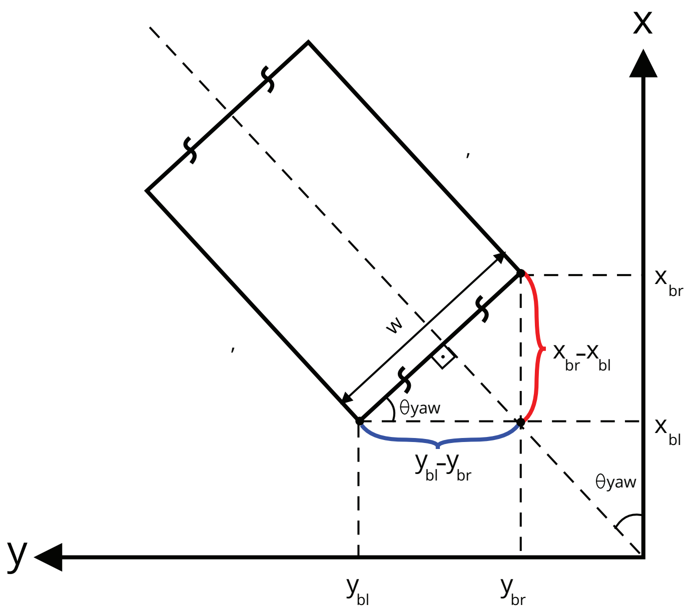

Figure 3.11: Geometric relation between (x_{br}, y_{br}) and (x_{bl}, y_{bl})

$$x_{fl} = -w \cdot sin\theta_{yaw} + x_{fr} \tag{3.18}$$

$$y_{fl} = w \cdot cos\theta_{yaw} + y_{fr} \tag{3.19}$$

Relative yaw angel value θ_{yaw-bl} can be calculated by Equation 3.20.

$$\theta_{yaw-br} = \begin{cases} \theta_{yaw} + 120 & \text{if}(-180 \leq \theta_{yaw} < 60) \\ \theta_{yaw} - 240 & \text{if } (60 \leq \theta_{yaw} \leq 180 \ ) \end{cases} \tag{3.20}$$

3.3.2 Link Blockage Check

We consider an intersection where radars mounted on the different vehicles are interacting with each other. Since there are no obstacles between the Tx radar on vehicle A and Rx radar on vehicle B, they establish LOS with each other as depicted in Figure 3.12(a). However, when another vehicle C drives to the intersection, it blocks the LOS, as illustrated in Figure 3.12(b). As a result, the detection loss happens in Rx radar.

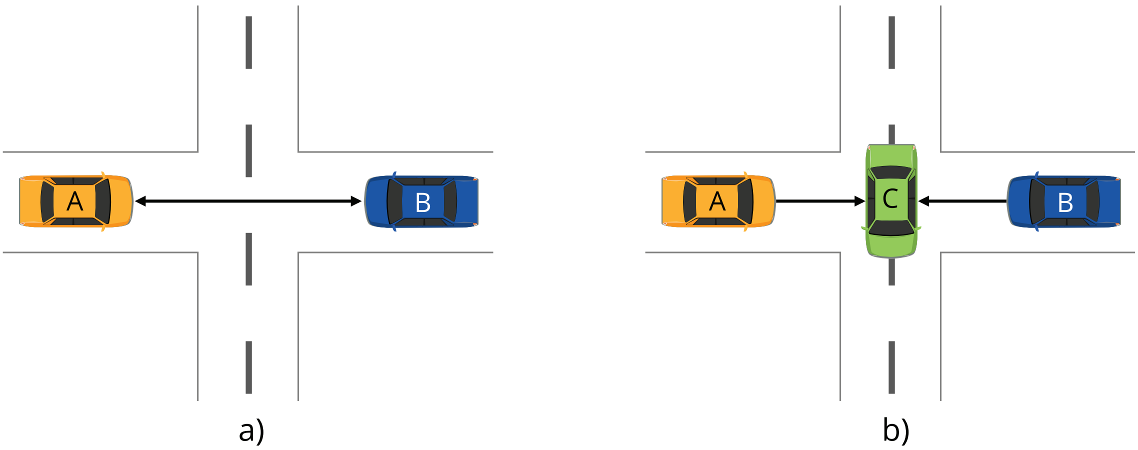

Figure 3.12: Illustration of link blockage between vehicles: a) no blockage b) blockage between vehicles

In our design firstly, we assume that if radar pairs are in each other's FOVs and there are no obstacles and a direct LOS is established as shown in Figure 3.12(a). Then, in order to identify blockage between radars, the outline of the vehicle is used as expressed in [45, 46] where if the transmitted signal from a radar intersects the outline points of the another vehicle between two facing radars, the link is considered non-LOS as shown in Figure 3.12(b) Finally, the set of LOS for each radar is obtained to be used in our study's next steps.

3.4 Wireless Channel Propagation Model

We chose simplified layer models to obtain feasible high-layer network simulations even though advanced channel propagation models are more commonly used to model all scatterers and reflectors in a vehicular environment. Having developed a network through joint radar communications in the mmWave band, we used ray-tracing models to model the channel. Consequently, our assumption was based on the theory that both radar and communication signals only propagate through a LOS path in case one exists, applying a geometry-based deterministic vehicular channel model. For simplification's sake, we ignored signals reflecting from the environment (ground, buildings) or other vehicles.

This simplified approach made it possible to receive three signals received by RadCom unit r_i from another r_j : the communication signal, the radar return, and the radar interference. We assumed that there was free space propagation conditions. With help of Equation 2.10, we calculated SNR captured by r_i for these there signals severally hereinbelow:

$$SNR_{\mathrm{r}} = \frac{P_r G_{trx} \lambda_r^2 \sigma G_{\mathrm{p}}}{N_r (4\pi)^3 d_{\mathrm{r}}^4}, \tag{3.21}$$

$$SNR_{\mathrm{int}} = \frac{P_r G_{trx} \lambda_r^2 G_{\mathrm{p}}}{N_r (4\pi)^2 d_{\mathrm{int}}^2}, \tag{3.22}$$

$$SNR_{\mathrm{c}} = \frac{P_c G_{trx} \lambda_c^2}{N_c (4\pi)^2 d_{\mathrm{c}}^2}, \tag{3.23}$$

Where σ denotes target's radar cross-section, G_{trx} is transmitter and receiver antenna gains (assuming that they are equal for all LOS), G_{p} states the radar processing gain. Since we work on both communication and radars systems, we have the separate wavelengths that are λ_{r} for radar signals, λ_{c} for communication signals respectively. Moreover, d_{r}, d_{int} and d_{c} stand for the sensing range for radar, the LOS interference range and the LOS communication range in turn. N_{r} and N_{c} are the noise powers caused by radar and communication systems' receivers and they are given by

$$N_r = B_r kTF \tag{3.24}$$

$$N_c = B_c kTF \tag{3.25}$$

Where B_{r} is radar bandwidth, k denotes Boltzman's constant, B_{c} is the communication bandwidth , F is the receiver's noise figure, and T in Kelvins is receiver temperature.

3.5 Enhancing VANET simulation with realistic Vehicular Mobility Traces

Simulation is the most effective way to evaluate the performance of a system in terms of time and cost. However, the results attained by simulation may not be reliable, depending on the vehicular topology designed. In the current simulation tools such as Matlab, SUMO, vehicular traffic scenario where vehicles move, is created by using a mobility model. A mobility model provides vehicle position information instantaneously, and a vehicular topology based on this information is unrealistically designed [47]. The obtained topology may give rise to unreliable results. Hence, it is crucial to acquire reliable results when evaluating the performance of the VANET. One particular method that stands out is to use real-time traffic data that includes vehicles' positions over time [47, 48]. Since the traffic data is taken at the certain time intervals, we need to fill the gaps between measurements. The movement of a vehicle, including its position information, can be described as a continuous function and the gaps can be filled by sampling the data. However, it is possible to lose a part of the data because of the low sampling rate. There are some ongoing studies to rebuild the vehicle's movement-based sampled trajectories by completing the lost data points. In [49] sampled signal is filtered to eliminate redundant points by keeping the essential ones and then pair each trajectory with a similar projection. Another study to rebuild a vehicle's trajectory is the interpolation method based on sequential records. For instance, the linear interpolation method is applied and elaborated in [50]. However, the linear interpolation method does not perform well in the trajectories, including curved paths. In [51], the proposed methodology contains two elements, which are reference system acquired by anchor points and a calibration method based on the reference system to acquire the missing points, respectively. [48] uses a clustering algorithm to complete the missing real data points in a vehicle trajectory. As a result of their studies, the Cologne trace provides the most comprehensive vehicular traces.

To evaluate the performance of our proposed RadCom approach, we used the vehicular mobility data set that [48] obtained as the result of their study. This study included the synthetic trace of vehicular traffic in Cologne at intervals of a minute for a total of 24 hours. We interpolated the data set by assuming the movement of a vehicle as a continuous function since RadCom units scan around at intervals of 10 μs. Then we simulated a realistic vehicular scenario, which is called Scenario-III, for the number of vehicles increasing from 4 to 12 at the steps of 4. Scenario-III included straight traffic without intersection where vehicles move straight and do not take any left or right. Hence, we had more straightforward traffic compared to Scenario-I and Scenario-II. The non-specific content and the massive size of the original data set constrained us from extracting more complex traffic situations. This problem was noted as an issue to deal with in future studies.

4

Enhanced RadCom Protocol for Mitigating Interference

The idea of increasing the amount of radars automotive radars deployed on a vehicle has been expected to result in a decrease in the detection performance since more interference occurs on the received signal. The real reason behind that is not to able to regulate the automotive radars present on a vehicle with the ones on the other vehicles appropriately. Therefore, this leads to not only an increase in mutual interference among radars but also to misdetection and ghost detection [4]. One solution to address mutual interference is RadCom. In this project, we utilized the RadCom protocol of [12, 9] to support the coordination of multiple FMCW radars placed on different parts of a vehicle, so that the field of view of these radars cover the whole region around the vehicle.

RadCom is supported by a MAC protocol to organize the channel usage with the different channel access method [12]. The resource allocation for radar and communication systems, the multiplexing scheme of radar signals, and channel usage schedule for vehicles are critical in designing a RadCom system [22]. We have used six radars for each vehicle and designed the resource allocation differently. Our RadCom protocol mainly consists of three parts, which are multiplexing, radar medium access control and communication medium access control.

4.1 Multiplexing

ADC in radar hardware has restraint on the choice of the waveform, and we use the same hardware for radar and communications systems. We need to pay attention to which waveform to use. For instance, joint waveform usage is not appropriate for RadCom because of ADC's limited performance. Besides, the usage of FMCW signals results in a quite low communication data rate [9]. Hence, in order to compensate for the limitation in ADC capabilities, we use multiplexing where the available frequency resource is allocated for two systems.

We selected FMCW as the waveform. Multiplexing in the frequency domain makes the system gain spectral efficiency and adaptability. Thereby, we split present radar hardware bandwidth B into four parts. The bandwidth for the communication unit(B_c) is 15 MHz. Also, we considered $B_c < 1/2T_s$ the relation between the sampling interval and the communication bandwidth. B_{LRR} and B_{MRR} are the bandwidths of long and medium-range radar units, and they are 800MHz, 250 MHz, respectively.

4.2 Radar Medium Access Control

If there are multiple vehicles equipped with the same type of radars transmitting simultaneously, or within a vulnerable period, then the effect of mutual interference on the radars' signal increases inevitably. That is why the dedicated channel needs to be appropriately shared among FMCW radars. The technique to achieve this is called radar time division multiple access (rTDMA) where radars are organized by alloting each a different rTDMA slots. We keep the bandwidth and carrier frequency values consistent during the transmission in order to reduce receiver complexity.

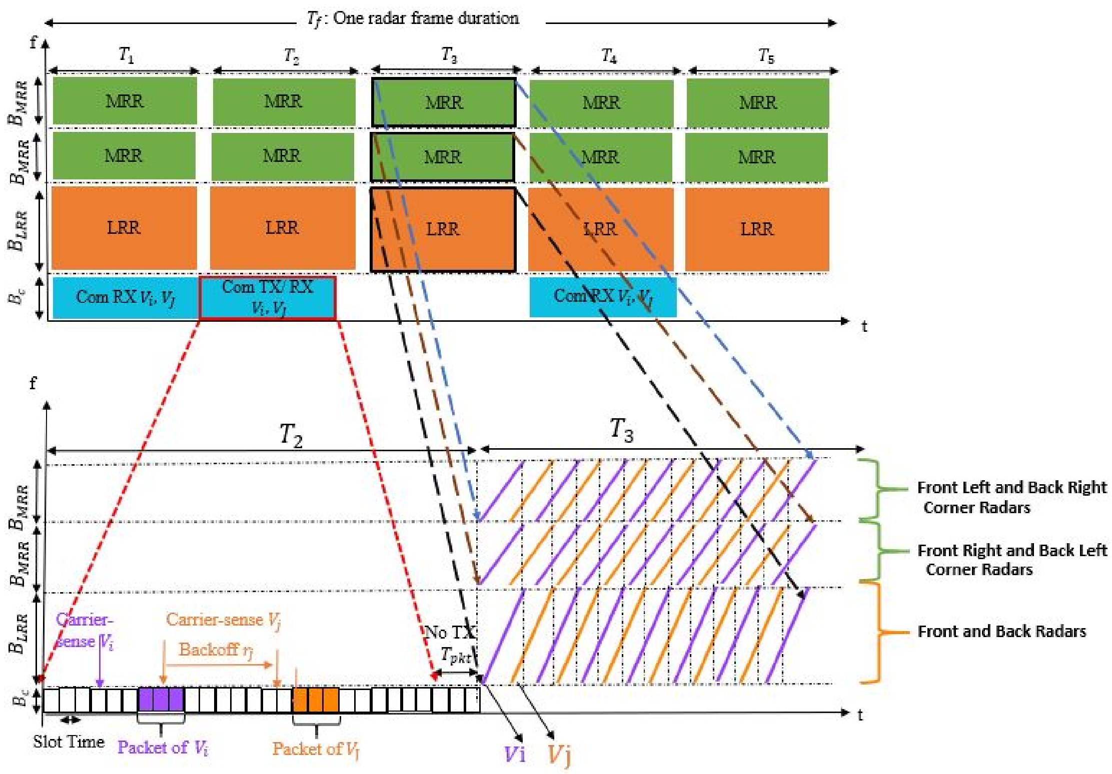

Figure 4.1: Illustration of frequency-time resources for the proposed RadCom. Scheduled radars by RadCom transmit within T_3

.

Let us consider a given Figure 4.1, which depicts how frequency and time division are achieved in our system. We split a radar frame T_f into 1/U time slots which are 5 [T_1, T_2,...T_5] in our design. Here, U as the modified radar duty cycle (Equation 4.1) is given by

$$U = (N + 1) \cdot T/T_f \tag{4.1}$$

Where $(N + 1) \cdot T$ denotes the duration of a one-time slot (Equation 4.2), and it equals to the sum of the duration of N chirps and one idle chirp time to prevent the chirps from overlapping. Also, by adding one idle chirp time, we can fit more than one chirp sequence for the radars on different vehicles into the same time slot. This slotted time is defined to get non-overlapping chirp sequences within a radar frame. As a result, mutual interference can be canceled or reduced to an acceptable level. N is the chirp sequence that radar will transmit, and it is 129 for LRR and MRR in our design. T_i and T are the duration of one-time slot and chirp duration in turn.

$$(N+1) \cdot T \leq T_i \tag{4.2}$$

The maximum number of radars that can transmits in the same time slot without interfering each other is $B_r/((1+\alpha_d) \cdot B_c)$. Where α_d denotes a constant value to take a direct link into account, which may lead to interference. It takes two separate values for LRR and MRR which are roughly 10 and 6, in turn.

To be able to take advantage of non-overlapping chirp sequences provided by rT-DMA slots, it is required to determine the maximum size of ($M_{\max}$) which represents how many vehicles can be fitted into available disjoint time- radar frequency source for mutual interference-free in a vehicular network [9]. $M_{\max}$ is given by [12]

$$M_{\max} \leq \frac{B_r}{(1+\alpha_d) \cdot B_c \cdot U} \tag{4.3}$$

The value of M is 25 and 95 respectively for LRR and MRR, and it means that we can schedule the radars of 25 vehicles without overlapping for LRR while schedule the radars of 95 vehicles without overlapping for MRR in a radar frame. Moreover, we used space-division multiple access (SDMA) to prevent two neighboring medium-range radars on the same vehicle from conflicting.

4.3 Communication Medium Access Control (cC-SMA)

The communication system in a RadCom unit has a significant impact on dealing with mutual interference because we use it to designate different time slots to radars seeing each other. A different frequency band is allocated for vehicular communication, and CSMA is responsible for organizing access to the shared communication channel. Since the topology in VANET updates dynamically, FDMA and TDMA are inadequate to control, and they require a central unit, as explained in Chapter 2. However, VANET does not support central units, so CSMA is the right choice for channel access control [38].

Every vehicle that intends to transmit their radar signals broadcast their control communication packets over a dedicated communication channel with CSMA with a random binary exponential backoff (BEB). Control communication packets are defined as broadcast messages, which do not require acknowledgment by RadCom units. It is a key player in mitigating interference.

We assume that all RadCom units on the same vehicle send the same control communication packet. Let us assume that vehicle i (V_i) has a chirp sequence transmission by using RadCom units through T_3 in T_f, broadcast a control communication packet (purple coloured rectangle) in T_2, which received by another vehicle j (V_j) as shown in Figure 4.1. A control packet has an identity (ID), Slot Index (SI), and the id-List, respectively. ID provides us information on the time reference [12]. All RadCom units on the same vehicle get the same ID, SI and id-List. SI denotes a randomly selected rTDMA slot index while the id-List keeps the list of vehicles having the same ID. Once a RadCom unit acquires the control communication packets from the neighboring vehicles, then redefines ID, SI, and id-List for its vehicle according to theirs without acknowledgement message. If V_j intends to transmit its chirp sequences in T_3, it declares by broadcasting its own control communication packet (orange coloured rectangle) in T_2. Note that its transmission is scheduled to a different and non-overlapping SI. Hence, V_j can transmit by using non-overlapping V_{per} after these arrangements by RadCom.

RadCom protocol enables a transmission schedule for the set of RadCom units of every vehicle, and it includes a distinct and compatible SI. If any clash of control packets occurs, it is solved in another radar frame with the help of [9]. Also, digital clock synchronization, which provides coordination among the vehicles, is done by GPS systems.

5

Results

The performance of the proposed radar communications protocol described in Chapter 4 for autonomous driving is evaluated in this chapter. In the following two sections, we explain the assumptions and simulation parameters; and then we discuss the acquired simulation results.

5.1 Simulation Parameters

To evaluate the performance of our proposed RadCom approach, firstly, we used our intersection designs in which vehicles were randomly (Scenario-I) and equally (Scenario-II) distributed among lanes. In every run of the first two scenarios, different vehicle topologies occur since our intersection design algorithms randomly create vehicle trajectories. Besides, vehicles approaching the intersection decelerate, they pass the intersection at $v = 30$ km/h and after passing the intersection they increase their speeds to $v = 50$ km/h again. After considering our virtual traffic scenarios, Scenario-III based on real-time traffic data, was used to examining the performance of proposed RadCom. A total of 10 Monte Carlo simulations of 6 s duration with the determined radar and communication parameters in Tables 5.1- 5.3 were done for all three scenarios, where the number of vehicles increasing from 4 to 16 at the steps of 4.

Table 5.1: Radar Simulation Parameters

Parameter	**Value**
LRR bandwidth (B_{LRR})	800 MHz
MRR bandwidth (B_{MRR})	250 MHz
ADC bandwidth (B_{ADC})	15 MHz
Carrier frequency (f_{LRR})	79.415 GHz
Carrier frequency (f_{MRR})	80.165 GHz
Modified duty cycle (U)	1/5
Vehicle radar cross section (σ)	10 dBsm
Radar transmitter power (P_{tx})	10 dBm
Radar processing gain (G_{p})	53.76 dB
Radar signal to noise ratio threshold (γ_{r})	3 dB
Chirp duration (T)	77.51 μs
Frame duration (T_f)	50 ms
Number of chirps per frame (N)	129

Table 5.2: Communication Simulation Parameters

Parameter	**Value**
Communication bandwidth B_c	15 MHz
Communication carrier frequency (f_c)	79.02 GHz
Packet size (N_{pkt})	100 Bytes
Modulation	16-QAM
Communication transmitter power (P_c)	23 dBm
Slot Time (δ)	10 μs
Maximum contention window size (W_0)	48
Maximum backoff stage (B)	3

Table 5.3: Joint Simulation Parameters for Both Radar and Communication

Parameter	**Value**
Maximum range of LoS interference for LRR and MRR	4-1 km (α_d =10-6)
Thermal noise temperature T_0	290 K
Receiver's noise figure F	10 dB
Antenna gain (G_{trx})	30-13 dBi
Antenna FOV for LRR	±10° (azimuth)
	±5° (elevation)
Antenna FOV for MRR	±75°(azimuth)
	±5° (elevation)

The dimensions of a Volvo XC90 [13] were chosen for vehicles' layout by assuming six RadCom units were mounted on a vehicle. LRR ones that use the same FMCW sawtooth radar waveform were placed above the windshields and rear window. In contrast, MRR ones that use the same FMCW sawtooth radar waveform placed above the right and left corners of the front and rear bumper. The values of elevation and the azimuth angels for front and rear RadCom units are ±5° and ±10°, respectively, whereas for the units on the corners are ±5° and ±75° in turn.

In our study, we selected ray-tracing models to model the channel. Both radar and communication signals are assumed only to propagate through a LOS path in case one exists for simplification, applying a geometry-based deterministic vehicular channel model. We ignored the signal reflected by the environment. The values of SNR received at RadCom units were calculated through Equation 2.10.

We formed the chirp sequence to satisfy the parameters of the detection system, which were introduced in Chapter 2.2. Maximum detectable range d_{max} takes distinct values for long and medium-range radars which are 200 m and 100 m respectively. Maximum unambiguously detected velocity v_{max} is 100 km/h. Range resolution is less than 1, and velocity resolution 0.5 severally. Also, we assigned two separate values to α_d, which states the existence of direct interferer since the proposed RadCom supports using both long and medium-range radars. It is possible to get a direct interference within 4 km for RadCom units with long-range functionality while within 1 km for ones with medium-range functionality.

Regarding the communication system, we assumed that communication links occur over AWGN for 16-QAM signals if the bit error rate (BER) were less or equal to 10^{-5}, in which case the achievable data rate was $2B_c$ based on the previous study [9].

5.2 Simulation Results and Discussions

This section elaborates on how the performance of the simulated RadCom for various inputs the number of vehicles, virtual and real traffic scenarios introduced in Chapter 3 by using different metrics.

5.2.1 The evaluation of Virtual Traffic Scenarios

To evaluate the performance of the RadCom protocol on traffic scenarios-I and II, we used different performance metrics.

One of the performance metrics is the fraction of radar blinds, which is described in [52] and given by Equation 5.1

$$F_{\mathrm{b}} = \frac{\text{the number of interfering RadCom units}}{\text{the total number of RadCom units}} \tag{5.1}$$

Figure 5.1 shows a comparison of the fraction of blinds for the number of vehicles (N_v) increasing from 4 to 16 at the steps of 4, for a total of 10 Monte Carlo simulations of 6 s simulation duration for Scenario-I and Scenario-II, and for the cases where RadCom was applied (RC) or not (NoRC). Note that, without RadCom, around 10 % of automotive radars are blinded by interference for the number of vehicles 4 in both scenarios. However, the ratio of blinded automotive radars increases proportionally by the number of vehicles. It fluctuates around 35% until 4.1 s, and then decreases for N_v=16 in Scenario-I. On the other side, it fluctuates around 41% until 2.6 s for N_v=16 in Scenario-II and then decreases. The reason for the decrease in interfering radars for both RC and NoRC is that vehicles are moving away from each other so the radars are not in each other's FOV.

When RadCom is applied, non-overlapping time slots are allocated for every RadCom unit in the system, and mutual interference can be canceled or reduced to an acceptable level. As a result, the fraction of radar blinds starts decreasing and reaches zero at different times, depending on the convergence time of the RadCom algorithm. The convergence time states the time for all RadCom units in a vehicular traffic scenario to reach negligible mutual interference. As shown in Figure 5.1, none of the RadCom units remains blinded for N_v= 4 and N_v=8 after their RadCom converged at different times, which are 38 ms and 60 ms in the Scenario-I. In comparison, they converged at 22 ms and 42 ms in the Scenario-II.

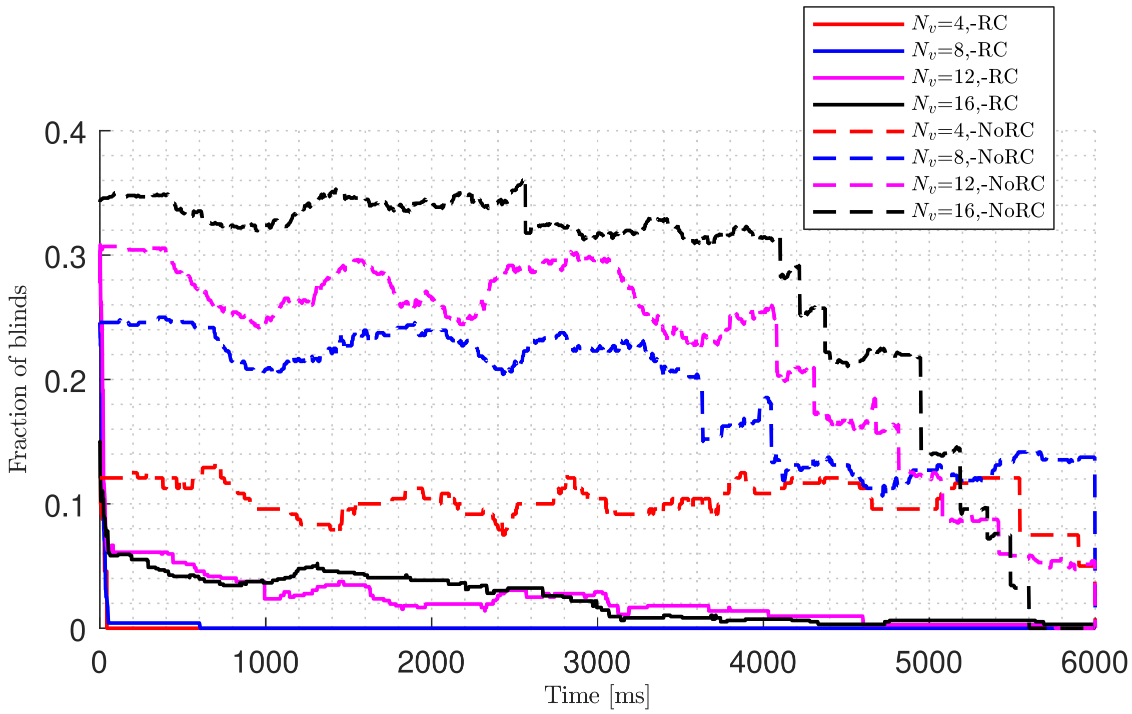

(a)

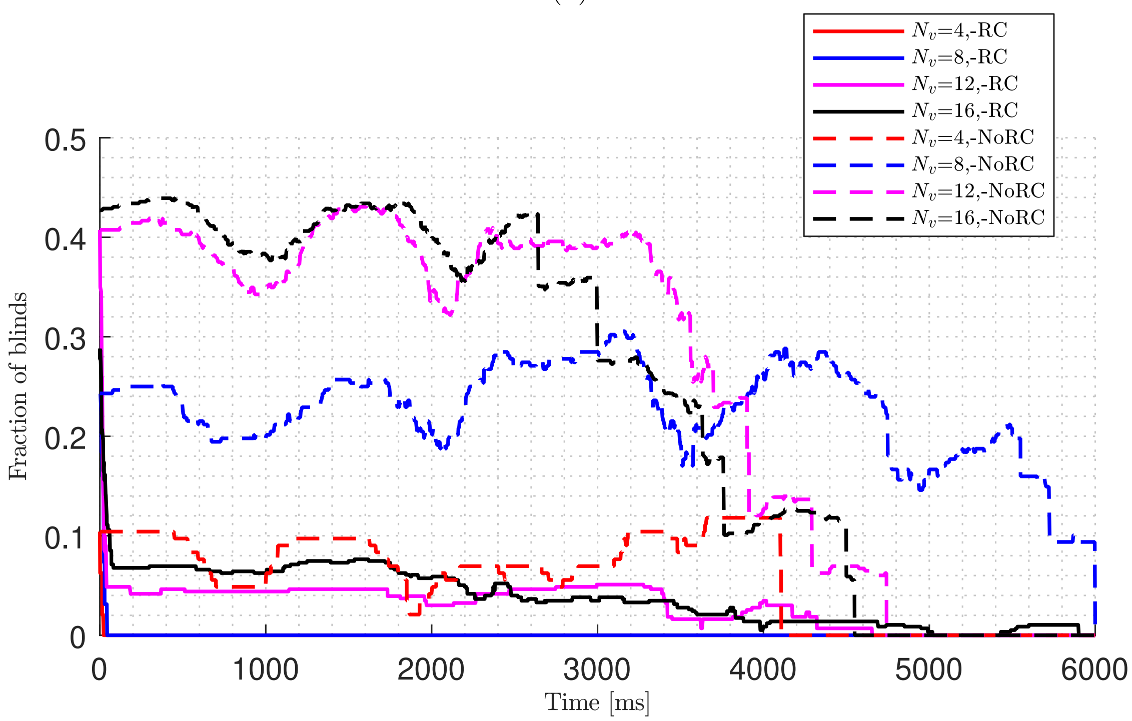

(b)

Figure 5.1: Comparison of the fraction of blinds with and without RadCom for $N_v = 4, 8, 12, 16$ a) Scenario-I and b) Scenario-II.

It takes a longer time to make all of the radars unblinded when N_v increases to 12, then to 16 in both scenarios. The reason behind it is that the RadCom algorithm keeps resolving the conflict and the interference occurred because of varying vehicular topology and the increased number of radars due to the increased number of vehicles. Hence, as soon as the proposed RadCom is initiated, the ratios of blinded automotive radars for varying vehicular topologies have considerably reduced compared to the ones without RadCom. As Figure 5.1 reveals, the fractions of blinds for N_v 16 in both scenarios remain below 10 percent until 4.6 s and 5 s in turn. Then, in both scenarios, the fractions reach zero eventually. Comparing both scenarios for the varying number of vehicles, the proposed RadCom shows a bit better performance for Scenario-II in terms of the fraction of radar blinds.

Another performance metric is the data rate per RadCom unit. Since the vehicular network topology varies continuously for both scenarios, the achieved data rate changes through time. That's why we evaluated the communication capability of the proposed RadCom, which is described as the function of time for varying N_v.

Figure 5.2 shows the data rate per node for a total of 10 Monte Carlo simulations of 6 s simulation duration of Scenario-I and Scenario-II. Since the main task of RadCom is to coordinate radar interference by assigning non-overlapping time slots to radars when it is initiated, RadCom protocol uses the most of available resource to perform this task. This process takes minimum and maximum about 5 ms-3 s in Scenario-I and 2.3 ms-0.5 s in Scenario-II respectively as N_v increases from 4 to 16. Hence, the data rate starts low and then increases. The maximum achieved data rate increases from approximate 13 Mbps to 17 Mbps at 51ms in scenario-I while it increases from approximate 13 Mbps to 21 Mbps at 51ms for N_v from 4 to 8. In Scenario-II the data rate for N_v=4 becomes zero at 4.2 s since vehicles are moving away from each other so RadCom units are no longer in each other's communication FOV. When it comes to N_v=12, the data rate per node starts increasing at 41ms-50ms and then takes the maximum approximate value 21 and 22 Mbps at 4.8 s- 4.7 s in turn in both scenarios. However, the achieved data rate for N_v=16 turns out to be 10 Mbps at 3.7 s in Scenario-I ,and 17 Mbps at 4.75 s in Scenario-II.

As seen from the data rate curves in the Figure 5.2, the maximum achieved data rate values for N_v from 4 to 12 are almost the same, but the time to reach the maximum one is a few ms shorter in Scenario-II than Scenario-I. In comparison, the maximum achieved data rate for N_v=16 is lower than the ones for N_v=8-12 ,and it is 17 Mbps in Scenario-II. The reason behind that is the dynamic of vehicular topology. Since Scenario-II consists of vehicles equally distributed on the lanes of the four-way intersection, it gets easier to coordinate the radar interference. Comparing both scenarios for the varying number of vehicles, we can say that the proposed RadCom shows a bit better and steady performance for Scenario-II from the viewpoint of the data rates per RadCom unit.

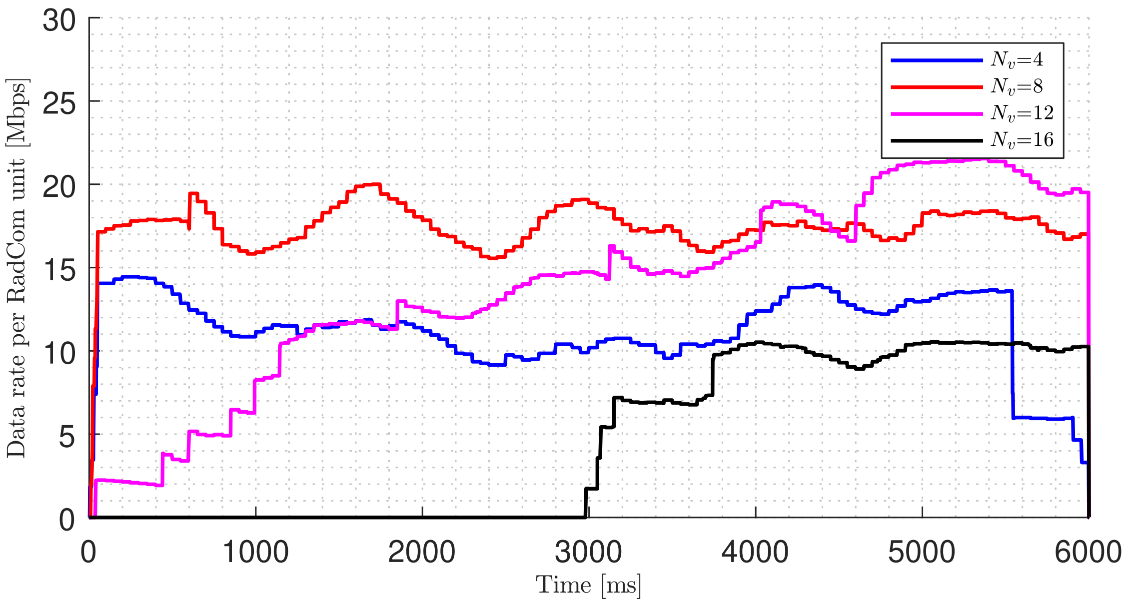

(a)

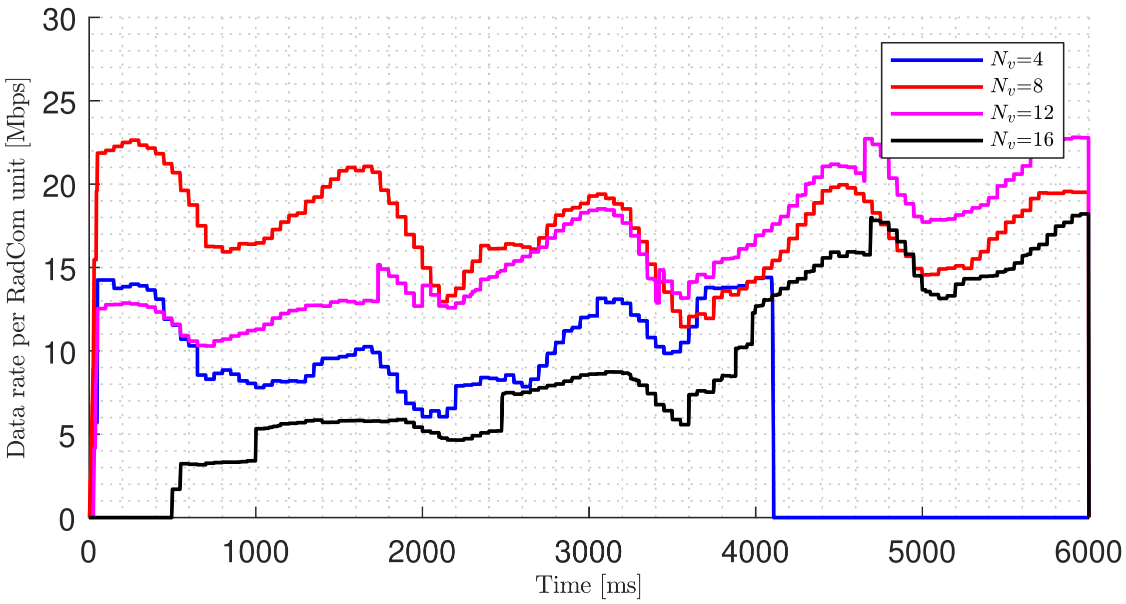

(b)

Figure 5.2: Communication data rate per RadCom unit for $N_v = 4, 8, 12, 16$ a) Scenario-I and b) Scenario-II.

As explained before, convergence time is the required time for all RadCom units in a vehicular traffic scenario to overcome and reach acceptable mutual interference. When all RadCom units converge, we get a fully connected, distributed, and vehicular network. Hence, convergence time t_{final} is a useful metric to evaluate the influence of varying vehicular topology with varying N_v on the proposed RadCom protocol.

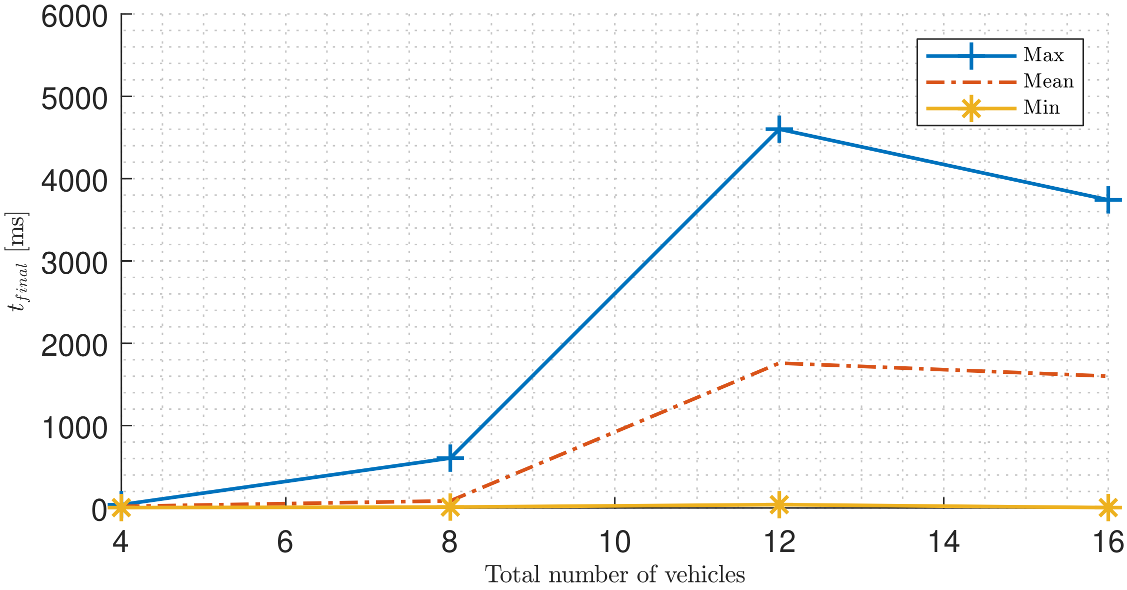

(a)

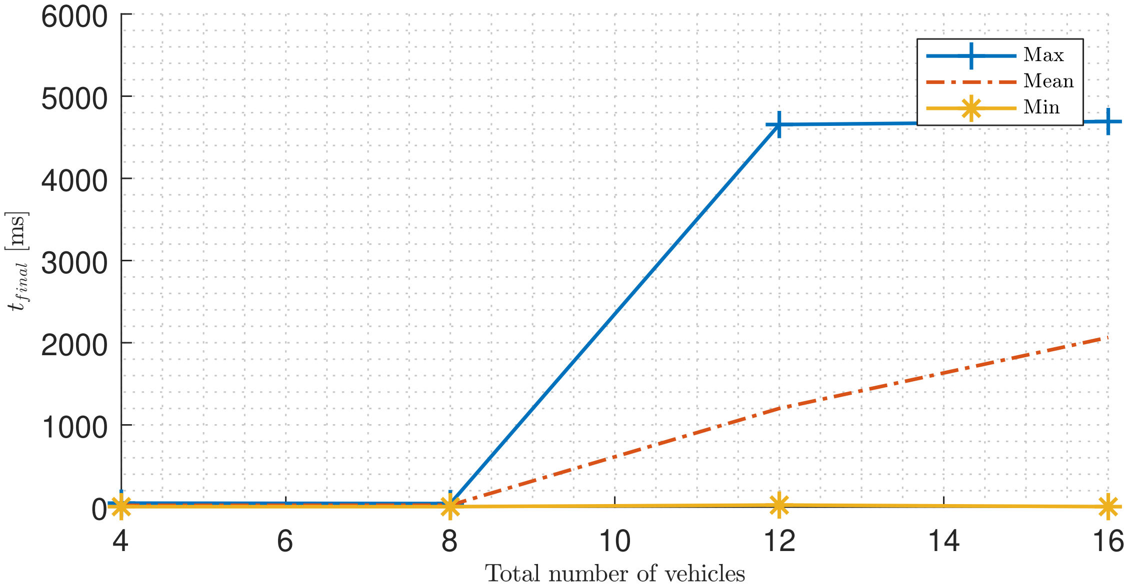

(b)

Figure 5.3: Maximum, mean and minimum time to reach negligible mutual interference for $N_v = 4, 8, 12, 16$ a) Scenario-I and b) Scenario-II.

Figure 5.3 shows the maximum, mean, and minimum values, which t_{final} takes for a total of 10 Monte Carlo simulations of 6 s simulation duration of Scenario-I and Scenario-II. As seen from the Figure 5.3, Max, $Mean$, and Min increase for varying N_v from 4 to 12 at the steps of 4 in both scenarios. For instance, in Scenario- I for N_v =12, they turn out to be 4.6 s, 1.8 s and 40 ms while are 4.7 s, 1.24 s and 25 ms in Scenario-II. However when N_v=16, Max, $Mean$ and Min decrease in Scenario-I. In contrast, Max, remains constant, $Mean$ increases slightly, and Min decreases in Scenario-II. The reason for this difference between the two scenarios is diversifying vehicular topology. In Scenario-I, it is highly possible to have complex traffic in which vehicles located in separate groups because of randomly distributed vehicles, whereas Scenario-II provides more regular traffic by equal distribution. Hence, it gets harder to achieve a fully connected vehicular network since it takes a longer time for RadCom protocol to coordinate all units in Scenario-I compared to Scenario-II. The simulations supports this claim. When we consider the output of the simulations for N_v =16, out of 50 % of ten simulations, we observe that RadCom protocol could not form a connected network for 6 s simulation duration, and t_{final} becomes zero. This means that, RadCom protocol can not converge and form a fully connected vehicular network. Scenario-II could form a fully connected vehicular network in 80 % of ten simulations resulting with non-zero t_{final}. Also, this observation explains the reason for unsteady changes on the values of Max, $Mean$ and Min for N_v =16. As the comments on the simulations' output and the given Figure 5.3 reveal, the proposed RadCom shows better performance in smaller vehicular topologies.

The proposed RadCom protocol allows us to see separately how long time it takes for each vehicle to converge in a fully connected vehicular network, and it is denoted by $t_{FinalEach}$. Figure 5.4 shows the maximum, mean, and minimum values, which $t_{FinalEach}$ takes for a total of 10 Monte Carlo simulations of 6 s duration for Scenario-I and Scenario-II, where N_v increasing from 4 to 12 at the steps of 4. Also, we separately discussed below $t_{FinalEach}$ for N_v =16, in order to resolve N_v easier for below 16. As seen in Figure 5.4 (a), Max, $Mean$, Min are increasing for N_v from 4 to 12 in Scenario-I. They turn out to be 740, 435, and 23 ms for N_v=12 in turn. As seen in Figure 5.4 (b) in Scenario-II, Min is decreasing from 21 to 17 ms for N_v from 4 to 12. Whereas Max and $Mean$ are increasing for N_v from 4 to 12 and turn out to be 31 and 27 ms, respectively. For N_v=12, they are remarkably shorter compared to the ones in Scenario-I. Since RadCom protocol could not form a fully connected network in some of the simulations, the obtained values are not reliable enough in both scenarios where N_v=16. The observed maximum, mean and minimum values for N_v from 4 to 12, state the impact of dynamically changing topology on the time when all RadCom units on each vehicle to converge in a fully connected vehicular network. Besides, comparing both scenarios, it can be said that the proposed RadCom shows a better performance for Scenario-II in terms of $t_{FinalEach}$, since it provides a traffic scenario where the vehicles are distributed equally.

After RadCom protocol of every vehicle resolves interference by assigning non-overlapping time slots to the radars, each vehicle broadcasts a communication packet includes vehicle trajectory information. Hence, vehicles can communicate with each other, and two vehicles that don't have contact with each other can have the trajectory information by a third one. For instance, in a scenario where three vehicles move on the same lane, vehicle 1 and vehicle 3 could have each other's trajectory information by vehicle 2, which moves in between the other two vehicles.

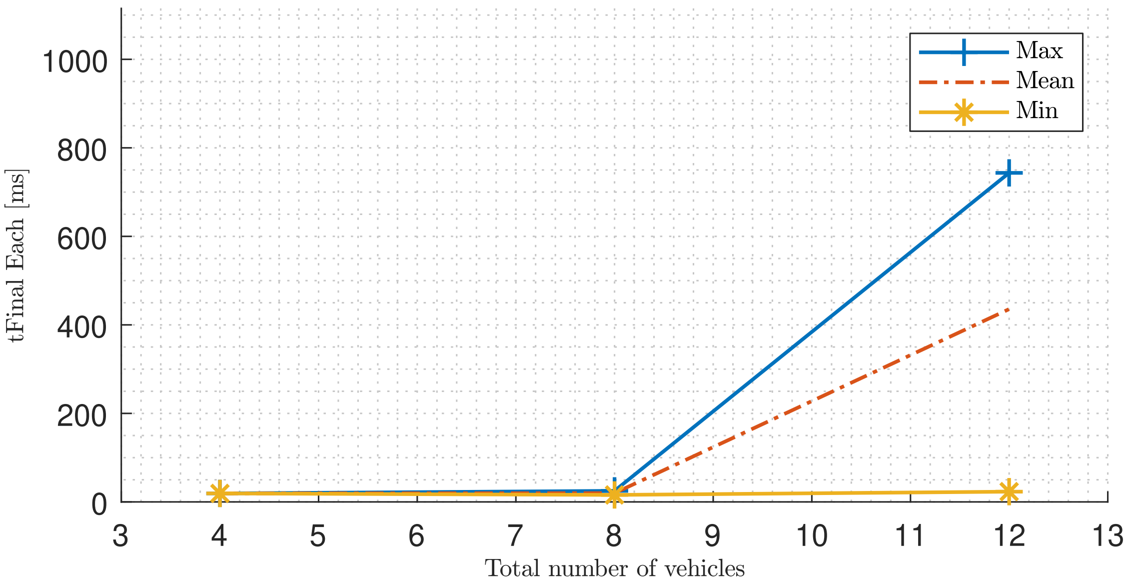

(a)

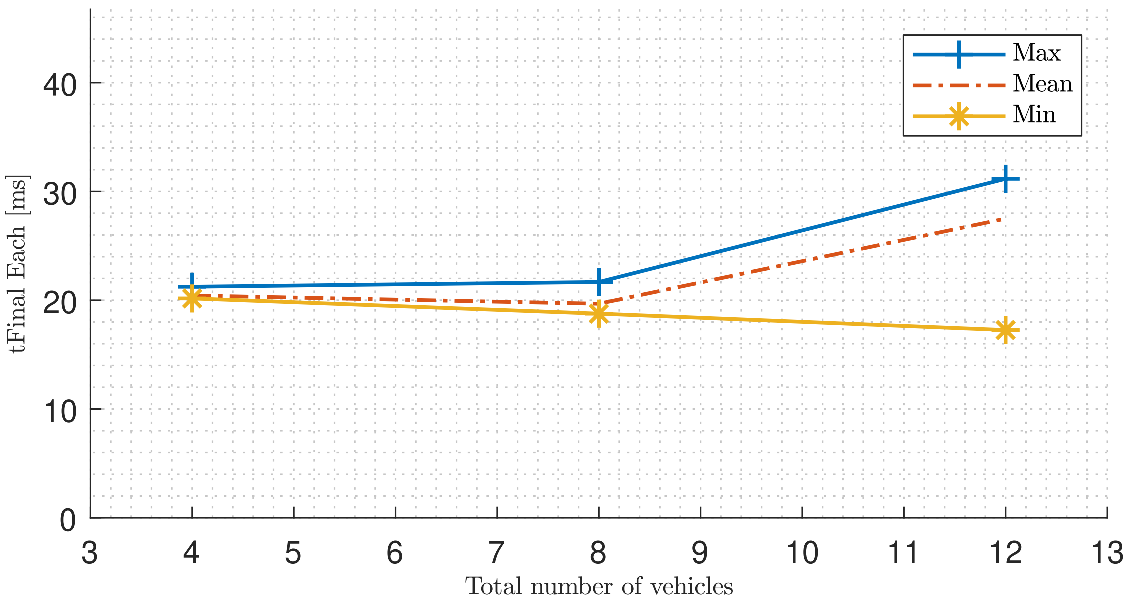

(b)

Figure 5.4: Maximum, mean and minimum values of $t_{FinalEach}$ for $N_v = 4, 8, 12$ a) Scenario-I and b) Scenario-II.

The delay time t_{Bcast} is how long time it takes to receive the communication packet broadcasted by a vehicle, which is a metric to evaluate the performance of RadCom protocol. Figure 5.5 shows the averaged values of t_{Bcast} and $t_{TFinalEach}$ take for a total of 10 Monte Carlo simulations of 6 s duration of Scenario I and Scenario-II, where N_v increasing from 4 to 12 at the steps of 4. We plotted them together since every vehicle broadcasts after converging in a fully connected network. Also, we excluded those simulation results for N_v =16 because of the reason explained below.

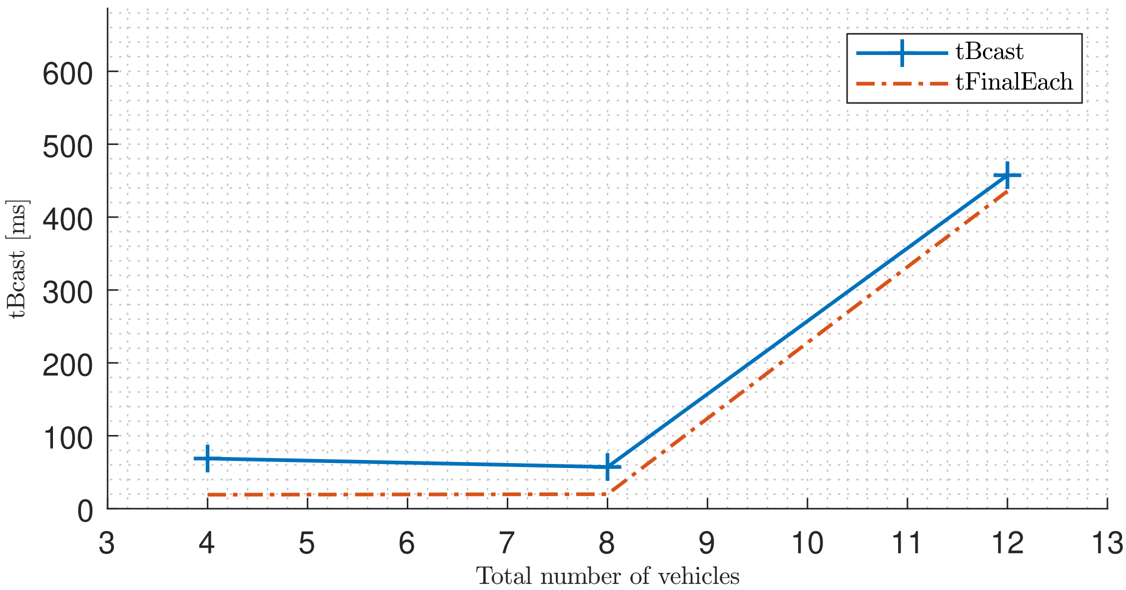

(a)

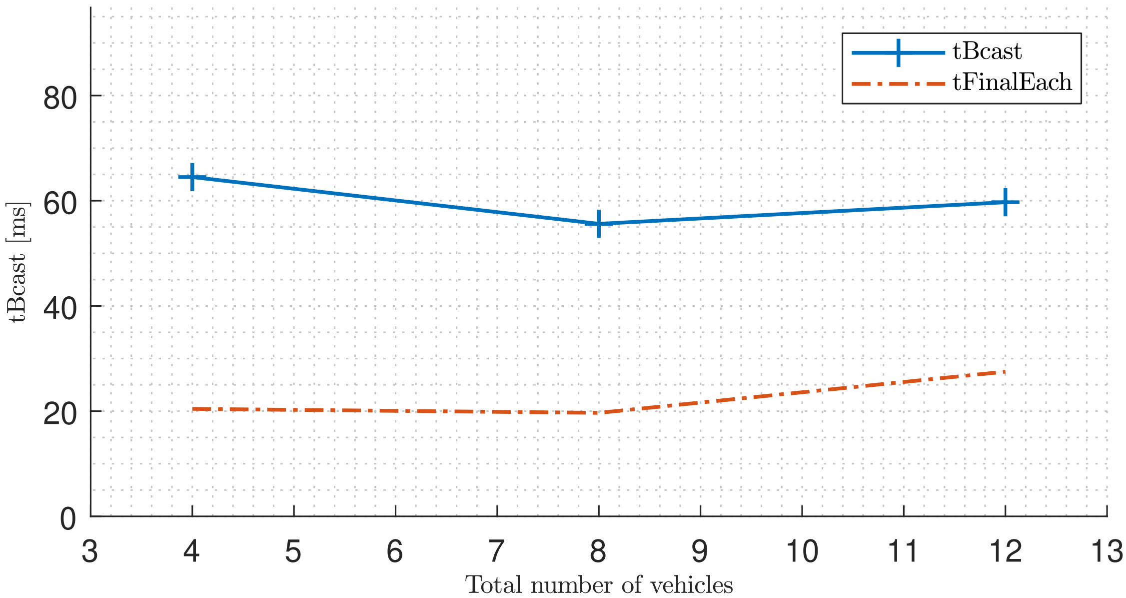

(b)

Figure 5.5: Averaged values of t_{Bcast} and $t_{TFinalEach}$ for $N_v = 4, 8, 12$ a) Scenario-I and b) Scenario-II.

In both scenarios, averaged $t_{TFinalEach}$ remains below averaged t_{Bcast}, and it means that each vehicle can reliably broadcast a communication packet after resolving interference. In Scenario-I, a vehicle broadcasts a communication packet, on average, 68 ms, but t_{Bcast} decreases to 57 ms for N_v from 4 to 8. In Scenario-II, t_{Bcast} decreases from 64 ms to 55 ms for N_v from 4 to 8. However, for N_v =12 t_{Bcast} increases to 460 ms in Scenario-I, while to 60 ms in Scenario-II. Also, for N_v =12 the averaged values of t_{Bcast} $t_{TFinalEach}$ is much smaller compared to the ones in scenario I. We determined an upper bound value (100 ms) to evaluate whether t_{Bcast} is at an acceptable level depending on scenario choice and the number of vehicles. If t_{Bcast} is higher than 100 ms, it means our proposed RadCom protocol based on the allocation of available resources, is inadequate to broadcast in acceptable delays. That is why we did not take the result from N_v =16 into account. However, we noted it as a future work to consider. As the observed values reveal, in Scenario-I, RadCom protocol could not manage to broadcast in acceptable delay for N_v =12 and 16 while in Scenario-II only for N_v =16. Besides, comparing both scenarios, it can be said that the proposed RadCom shows a better performance for Scenario-II in terms of t_{Bcast}, since it provides a traffic scenario, which is not sophisticated.

5.2.2 The evaluation of Realistic Traffic Scenario

The performance of the proposed RadCom based on the realistic vehicular mobility traces that was introduced in Chapter 3.5 to enhance VANET simulations is a critical metric to evaluate it. Hence, we followed the same steps in Scenario-I and Scenario-II for Scenario-III based on real-time traffic data. Scenario-III included straight traffic without intersection, where vehicles move straight and do not take any left or right as explained in Chapter 3.5. Hence, we had more simple traffic compared to Scenario-I and Scenario-II.

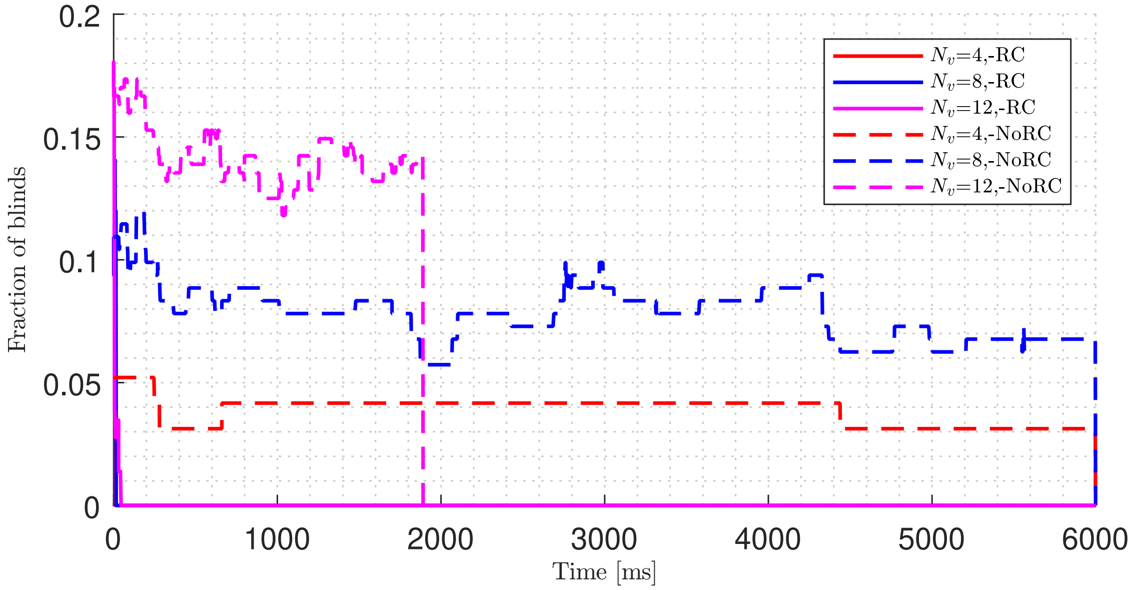

Figure 5.6: Comparison of the fraction of blinds with and without RadCom for $N_v = 4, 8, 12$ in Scenario-III.

Figure 5.6 shows a comparison of the fraction of blinds for the number of vehicles (N_v) increasing from 4 to 12 at the steps of 4, for a total of 10 Monte Carlo simulations of 6 s duration of Scenario-III and for the cases where RadCom was applied or not. Note that, without RadCom, the ratio of blinded automotive radars increases proportionally by the number of vehicles, and it varies between around 5 percent and 10 percent for the varying N_v 4 and 8. On the other side, for N_v=12 it fluctuates around 15 percent until 1.9 s, then becomes zero. The reason for the decrease in interfering radars in both cases is that vehicles are moving away from each other, so they do not interfere with each other, as explained in consideration of Scenario-I and Scenario-II. When RadCom is applied, the fraction of radar blinds starts decreasing and reaches zero at different times, depending on the convergence time of the RadCom algorithm. As shown in Figure 5.6, none of the RadCom units remains blinded for varying N_v after their RadCom converged at different times, which are 11.4 ms, 15 ms and 45.5 ms in turn. When comparing these values with the ones obtained in virtual scenarios, they are approximately three times shorter than the ones in Scenario-I. In contrast, they are twice as low as the ones in Scenario-II. The reason behind this is that the vehicles in Scenario-III drive straight, and the change in topology is much smaller compared to Scenario-I and Scenario-II.

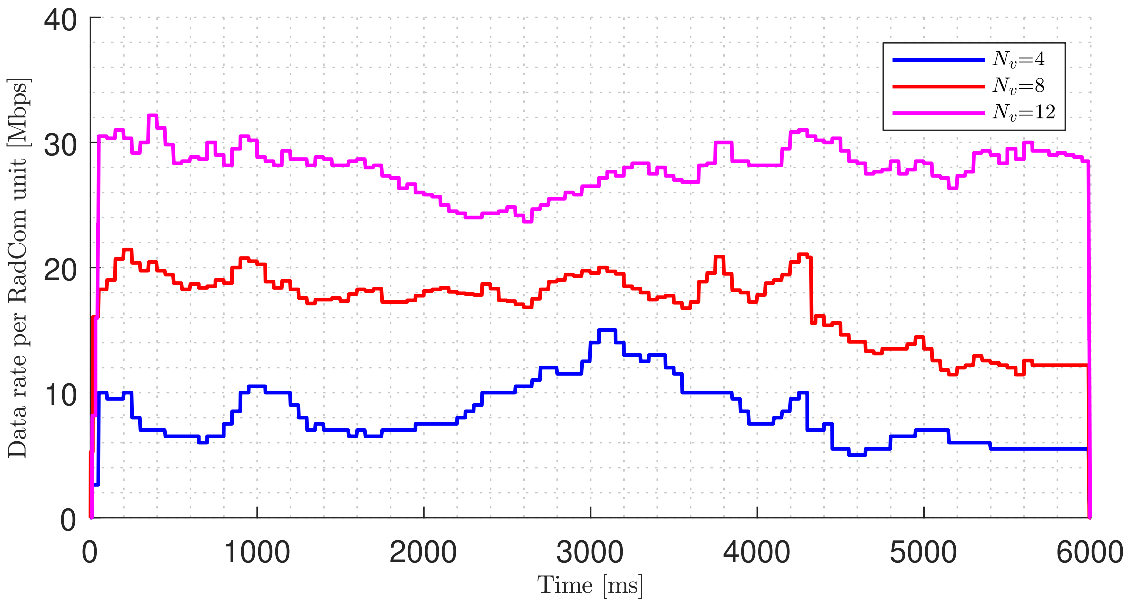

Figure 5.7: Communication data rate per RadCom unit for $N_v = 4, 8, 12$ in Scenario-III.

Figure 5.7 shows the data rate per RadCom unit (node) for a total of 10 Monte Carlo simulations of 6 s duration of Scenario-III. As explained before, it takes a slightly longer time to coordinate radar interference by assigning non-overlapping time slots to radars by RadCom protocol. This process takes a minimum of 0.6 ms and a maximum of 50 ms, respectively, for N_v increasing from 4 to 8, then to 12. Hence, the data rate starts low and then increases as occurred in the virtual scenarios. The maximum achieved data rate fluctuates at approximate 10 Mbps, 20 Mbps, and 30 Mbps for the vehicular groups of 4, 8, and 12. The maximum data rate values achieved in Scenario-III are slightly higher, and the times to reach it takes a much shorter time than the ones in Scenario-I and Scenario-II. RadCom shows a slenderly better and steady performance compared to the virtual scenarios from the viewpoint of the data rates per RadCom unit since the allocation of available resources requires less effort because of the topological advantage of Scenario-III.

Figure 5.8 shows the maximum, mean, and minimum values, which t_{final} takes for a total of 10 Monte Carlo simulations of 6 s duration of Scenario-III. As seen from the Figure 5.8, Max and $Mean$, decrease from 46.17 ms and 14.5 ms to 13.9 ms and 6.4 ms respectively for varying N_v from 4 to 8 at the steps of 4. However when N_v reaches 12, Max and $Mean$ increase to 42 ms and 23 ms in turn. In contrast, Min, remains constant during the simulation. These values are much less than the ones obtained in Scenario-I and Scenario-II. In Scenario-III, we have less complicated traffic where vehicles move on a straight path compared to virtual scenarios. Hence, it gets easier to achieve a fully connected vehicular network since RadCom protocol coordinates all units in a shorter time.

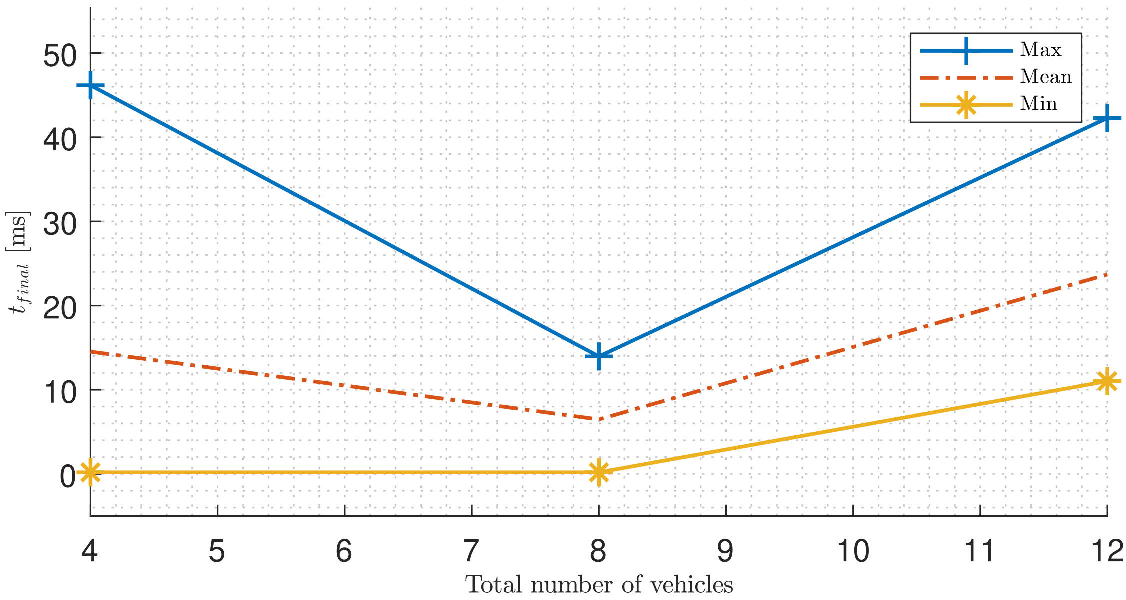

Figure 5.8: Maximum, mean and minimum time to reach negligible mutual interference for $N_v = 4, 8, 12$ in Scenario-III.

As we mentioned before, $t_{FinalEach}$ shows how long time it takes for all RadCom units on each vehicle to converge in a fully connected network, and it can be obtained by the output of RadCom protocol. Figure 5.9 shows the maximum, mean, and minimum values, which $t_{Final-Each}$ takes for a total of 10 Monte Carlo simulations of 6 s duration of Scenario-III, where N_v increasing from 4 to 12 at the steps of 4. As seen in Figure 5.9, Max, $Mean$, and Min for N_v=4 are 12 ms each. When N_v is 8, they decrease to 6, 5.7, and 4.4 ms in turn. However, when it comes to N_v =12, they increase to 8, 7.9, and 5.7 ms, respectively. We also investigated vehicle positions to understand the reason why those values were maximum for N_v =4, even though there was no complex traffic. The reason behind this is that most of the radars do not see each other due to the vehicles' direction. Besides, the observed values are smaller than the ones obtained in Scenario-I and Scenario-II. Comparing all scenarios, it can be said that the proposed RadCom shows a better performance for Scenario-III in terms of $t_{FinalEach}$.

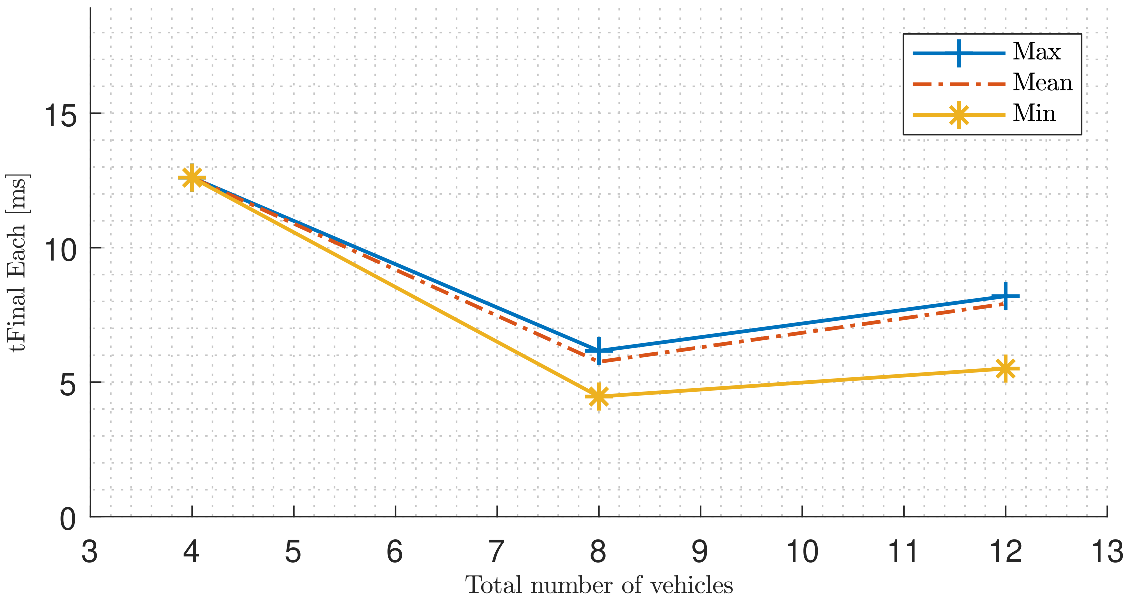

Figure 5.9: Maximum, mean and minimum values of $t_{FinalEach}$ for $N_v = 4, 8, 12$ in Scenario-III.

We explained in the previous section that the delay time t_{Bcast} is a critical metric to evaluate the performance of RadCom protocol. Figure 5.10 shows the averaged values of t_{Bcast} and $t_{TFinalEach}$ take for a total of 10 Monte Carlo simulations of 6 s duration of Scenario-III, where N_v increases from 4 to 12 at the steps of 4.

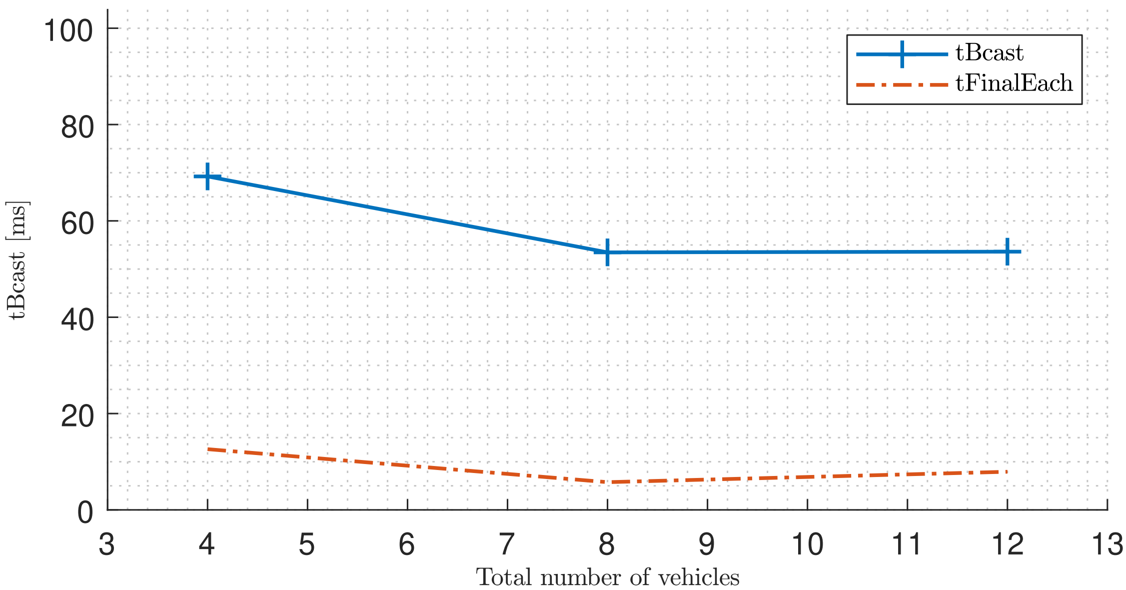

Figure 5.10: Averaged values of t_{Bcast} and $t_{TFinal-Each}$ for $N_v = 4, 8, 12$ in Scenario-III.

The averaged $t_{TFinal-Each}$ remains below averaged t_{Bcast}, and each vehicle can reliably broadcast its communication packet after resolving interference. As seen in Figure 5.10, the averaged values of t_{Bcast} and $t_{TFinalEach}$ vary by increasing N_v. t_{Bcast} and $t_{TFinalEach}$ are 70 ms and 12 ms in turn for N_v=4. When N_v is increased to 8, they decrease to 55 ms and 5.7 ms, respectively. When it comes to N_v=12 t_{Bcast} remains almost the same, while $t_{TFinalEach}$ increases to 7.9 ms. The reason behind that t_{Bcast} becomes maximum even though N_v becomes N_v=4 is that the vehicular topology. Also, LRR and MRR have different communication ranges, which shorter compared to the ones for radar ranges. Hence, most of RadCom units are not in each other's communication FOV due to the vehicles' direction and position in N_v=4 As the given figure reveals, our proposed RadCom protocol based on the allocation of available resources managed to broadcast in acceptable delays since all of the observed t_{Bcast} are smaller than 100 ms.Besides, comparing the observed results from scenario-I and scenario-II, it can be said that the proposed RadCom shows a better performance for Scenario-III in terms of t_{Bcast} since its topology does not dramatically.

6 Conclusion

This chapter summarizes the thesis and discusses the societal, ethical, ecological aspects, and the future works that weren't considered in the project.

6.1 Summary

We have proposed a distributed radar communication system for automotive applications in complex traffic scenarios. We modeled traffic scenarios including non-signalized intersections and real-time traffic data with the position traces of vehicles. The RadCom protocol of [12, 9] was extended so as to support the coordination of multiple FMCW radars placed on different parts of a vehicle so that the field of view of these radars form a whole region around the vehicle.

Firstly, we investigated the performance of our proposed RadCom protocol in dynamically varying traffic based on complex traffic scenarios. They consisted of four-way intersections with straight, right-left- turn traffic, where vehicles were randomly distributed (Scenario-I) and equally distributed (Scenario-II) among lanes. The evaluation results were represented by comparing the simulated performance of RadCom by using various metrics. RadCom protocol converged in less than 4.7 s, the achieved data rates increased with the number of vehicles N_v from 4 to 12. The maximum achieved data rates in Scenario-I and Scenario-II were 21 Mbps and 22 Mbps in turn for N_v=12. In comparison, the achieved data rates decreased to 10 Mbps in Scenario-I and 17 Mbps in Scenario-II, respectively, for N_v=16. The fraction of blind radars became zero in less than 60ms for $N_v = 4, 8$ while this time increased with varying N_v from 12 to 16. However, it took a long time to make the radars unblinded; the ratios of unblinded radars with RadCom were very low compared to the ones without RadCom for N_v from 12 to 16 in both scenarios.

Moreover, the proposed RadCom protocol allowed us to see separately how long time it took for each vehicle to converge in a fully connected vehicular network. This time increased depending on the number of vehicles and vehicular topology in scenarios. It was between, on average, 20 ms and 435 ms in Scenario-I while 20 ms and 27 ms in Scenario-II. Besides, we considered the delay in the time of every vehicle to broadcast a communication packet. This delay varied depending on the complexity of vehicular topology. RadCom protocol was able to achieve broadcasting the communication packet between in 68 ms and 57 ms for N_v=4,8 in Scenario-I, whereas between 64 ms and 60 ms for N_v=4,12 in Scenario-II. However, it was observed from corresponding simulations that the delay time of the communication packet was not at the acceptable level for the case where N_v=12,16 in Scenario-I while N_v=16 in Scenario-II. The reason behind the long delay times was that the proposed RadCom protocol based on the allocation of available time and frequency resources was so sensitive to the changes in the complexity of vehicular topology. Thereby, it could not broadcast within the acceptable delay.

Additionally, when we applied the RadCom protocol to real-time traffic (Scenario-III) based on real-time traffic data set, the obtained results from the simulations were found to be better than the ones for Scenario-I and Scenario-II. The maximum data rate per RadCom unit was 30 Mbps, and the ratio of blinded radars reached zero in 45.5 ms for N_v=12. Besides, the RadCom protocol converged in less than a maximum of 42 ms. Moreover, the averaged delay time of communication packets was very close to the ones in Scenario-II for N_v varying from 4 to 12.

Scenario-I and Scenario-II were based on virtual mobility models as described Chapter 3.1 and provided complex traffic scenarios based on dynamically changing vehicular topologies. These topologies were considerably complicated since they covered going straight, left, and right-turning vehicles on the intersection. In contrast, the ones in scenario-III went straight without turning on the road, as described in Chapter 3.5. The resource consisting of well-organized realistic traffic data was not satisfactory, and it took much time to extract reliable data sets and interpolate by tiny time intervals from the existing data sets. Hence, Scenario-I and Scenario-II, compared to Scenario-III, provided realistic results that we could encounter in real highway traffics.

6.2 The Societal, Ethical, Ecological Aspects of The Thesis Project

This thesis aimed to improve an existing RadCom protocol to be used for mitigating mutual interference in complex virtual and real-time traffic scenarios. Since the same radar hardware is used for V2V communication too, this does reduce not only hardware cost but also provides efficiency in the usage and allocation of available time and frequency resources.

The proposed RadCom protocol achieved mitigating mutual interference among faced radars in complex traffic scenarios. So, vehicles and drivers would be expected to benefit from it in terms of autonomous driving, traffic coordination, and collision avoidance.

Also, the results of this thesis were discussed in terms of public health and the environment. According to the World Health Organization (WHO), there is no concrete evidence regarding the negative impact of exposure to RF signals on human health, at or below the upper limit by international standards [53]. Nevertheless, WHO states that in order to provide more specific data, more research should be carried out.

Autonomous driving is getting more attention since it undertakes some responsibilities of drivers so that they might devote much more time to do other things during traveling. However, some cases can require the driver's sudden control and quick decision. In this thesis, vehicles are still under the control of drivers, and RadCom is responsible for nothing related to maneuvering the vehicle. Also, neighboring vehicles are aware of each other's movements, thanks to RadCom, which reduces the possibility of traffic congestion and collision, but increases traffic safety and efficiency.

6.3 Further Work

Future work shall consider channel modeling based on a ray-tracing model, including reflections from the environment, more realistic vehicular kinematics such as acceleration and deceleration. Also, it is vital to decrease communication delays to acceptable levels by adapting the RadCom protocol to changing conditions.

Bibliography

[1] Macrovectors, “Smart City Traffic,” https://www.freepik.com/free-vector/smart-city-traffic-isometric_5972706.htm, 2020, [Online; accessed 25-May-2020].

[2] L. Chen and C. Englund, “Cooperative intersection management: A survey,” in *IEEE Transactions on Intelligent Transportation Systems*, vol. 17, no. 2, 2016, pp. 570–586.

[3] L. Y. H. W. Lin, J., “Design of an fmcw radar baseband signal processing system for automotive application,” *SpringerPlus*, 2016. [Online]. Available: https://doi.org/10.1186/s40064-015-1583-5

[4] Y. Han, E. Ekici, H. Kremo, and O. Altintas, “Automotive radar and communications sharing of the $79ghz$ band,” in *Proceedings of the First ACM International Workshop on Smart, Autonomous, and Connected Vehicular Systems and Services*, ser. CarSys ’16. New York, NY, USA: Association for Computing Machinery, 2016, p. 6–13. [Online]. Available: https://doi.org/10.1145/2980100.2980106

[5] K. Sjoberg, P. Andres, T. Buburuzan, and A. Brakemeier, “Cooperative intelligent transport systems in europe: Current deployment status and outlook,” *IEEE Vehicular Technology Magazine*, vol. 12, no. 2, pp. 89–97, 2017.

[6] M. Zhonga, Y. Yangb, Y. Dessoukyc, and O.Postolached, “Multi-agv scheduling for conflict-free path planning in automated container terminals,” *ELSEVIER Computers Industrial Engineering*, vol. 142, April 2020. [Online]. Available: https://doi.org/10.1016/j.cie.2020.106371

[7] X. Xia, X. Ma, and J. Wang, “Control method for signalized intersection with integrated waiting area,” *The Application of Sliding Mode Control in Robots*, March 2019.

[8] Y. Zeng, Y. Ma, and S. Sun, “Joint radar-communication with cyclic prefixed single carrier waveforms,” *IEEE Transactions on Vehicular Technology*, vol. 69, no. 4, pp. 4069–4079, 2020.

[9] C. Aydogdu, N. Garcia, and H. Wymeersch, “Radar communication for combating mutual interference of fmcw radars,” in *IEEE Global Communications Conference (GlobeCom)*, 2018. [Online]. Available: https://arxiv.org/abs/1807.01497

[10] J. Shaw, “Intersection Safety Issue Briefs,” https://safety.fhwa.dot.gov/intersection/other_topics/fhwasa10005/brief_2.cfm/, 2020, [Online; accessed 25-May-2020].

[11] S. Rao, "Intro to mmwave sensing: Fmcw radars - module 1 : Range estimation," Jun 2018. [Online]. Available: https://training.ti.com/intro-mmwave-sensing-fmcw-radars-module-1-range-estimation?cu=1128486

[12] C. Aydogdu, M. F. Keskin, N. Garcia, H. Wymeersch, and D. W. Bliss, "Radchat: Spectrum sharing for automotive radar interference mitigation," *IEEE Transactions on Intelligent Transportation Systems*, p. 1–14, 2019. [Online]. Available: http://dx.doi.org/10.1109/TITS.2019.2959881

[13] Volvo, "Volvo XC90 Dimensions," https://www.volvocars.com/intl/cars/new-models/xc90/specifications/dimensions, 2020, [Online; accessed 25-May-2020].

[14] F. Zhang, Z. Zhang, W. Yu, and T. Truong, "Joint range and velocity estimation with intrapulse and intersubcarrier doppler effects for ofdm-based radcom systems," *IEEE Transactions on Signal Processing*, vol. 68, pp. 662–675, 2020.

[15] U. K. Singh, R. Mitra, V. Bhatia, and A. K. Mishra, "Kernel lms-based estimation techniques for radar systems," *IEEE Transactions on Aerospace and Electronic Systems*, vol. 55, no. 5, pp. 2501–2515, 2019.

[16] M. Braun, C. Sturm, and F. K. Jondral, "Maximum likelihood speed and distance estimation for ofdm radar," in *2010 IEEE Radar Conference*, 2010, pp. 256–261.

[17] Y. Zeng, Y. Ma, and S. Sun, "Joint radar-communication: Low complexity algorithm and self-interference cancellation," in *2018 IEEE Global Communications Conference (GLOBECOM)*, 2018, pp. 1–7.

[18] T. Huang and T. Zhao, "Low pmepr ofdm radar waveform design using the iterative least squares algorithm," *IEEE Signal Processing Letters*, vol. 22, no. 11, p. 1975–1979, Nov 2015. [Online]. Available: http://dx.doi.org/10.1109/LSP.2015.2449305

[19] B. Schweizer, C. Knill, D. Schindler, and C. Waldschmidt, "Stepped-carrier ofdm-radar processing scheme to retrieve high-resolution range-velocity profile at low sampling rate," *IEEE Transactions on Microwave Theory and Techniques*, vol. 66, no. 3, pp. 1610–1618, 2018.

[20] Y. Liu, G. Liao, and Z. Yang, "Robust ofdm integrated radar and communications waveform design based on information theory," *Signal Processing*, vol. 162, p. 317–329, Sep 2019. [Online]. Available: http://dx.doi.org/10.1016/j.sigpro.2019.05.001

[21] P. Kumari, J. Choi, N. González-Prelcic, and R. W. Heath, "Ieee 802.11ad-based radar: An approach to joint vehicular communication-radar system," *IEEE Transactions on Vehicular Technology*, vol. 67, no. 4, pp. 3012–3027, 2018.

[22] V. Petrov, G. Fodor, J. Kokkoniemi, D. Moltchanov, J. Lehtomaki, S. Andreev, Y. Koucheryavy, M. Juntti, and M. Valkama, "On unified vehicular communications and radar sensing in millimeter-wave and low terahertz bands," *IEEE Wireless Communications*, vol. 26, no. 3, pp. 146–153, 2019.

[23] S. Baskar and E. Ertin, "A software defined radar platform for waveform adaptive mimo radar research," in *2015 IEEE Radar Conference (RadarCon)*, 2015, pp. 1590–1594.

[24] H. T. C. Wu, W. Yang and J. Wang, "Traffic pattern modeling, trajectory classification and vehicle tracking within urban intersections," *2017 International Smart Cities Conference (ISC2)*, pp. 1–6, Sept 2017.

[25] J. W. H. X. D. Tian, Y. Yuan and J. Wang, "Collision avoidance on winding roads using dedicated short-range communication," *Transpor*, vol. 33, 2018. [Online]. Available: https://journals.vgtu.lt/index.php/Transport/article/view/176

[26] S. Stephenson, "Network rtk for intelligent vehicles: Accurate, reliable, available, continuous positioning for cooperative driving," *GPS World*, vol. 24(2), pp. 61–67, 2013.

[27] K. N. Qureshi, A. H. Abdullah, R. W. Anwar, and F. Ullah, "A systematic review on routing protocols of vehicular ad hoc networks," *KSII The 7th International Conference on Internet (ICONI)*, Dec 2015.

[28] A. Daniel, A. Paul, A. Ahmad, and S. Rho, "Cooperative intelligence of vehicles for intelligent transportation systems (its)," *Springer Wireless Pers Commun.*, no. 87, pp. 464–484, 2015.

[29] S. Wanga, W. Huanga, and H. K. Loa, "Traffic parameters estimation for signalized intersections based on combined shockwave analysis and bayesian network," *ELSEVIER Transportation Research Part C*, pp. 22–37, May 2019.

[30] X. Zhao, J.Wang, G. Yin, and K. Zhang, "Cooperative driving for connected and automated vehicles at non-signalized intersection based on model predictive control," *2019 IEEE Intelligent Transportation Systems Conference (ITSC)*, pp. 2121–2126, Oct 2019.

[31] M. I. Skolnik, *Radar Handbook*, 3rd ed. New York: McGraw-Hill Education, 2008.

[32] C. Wolff, "Radar basics." [Online]. Available: http://www.radartutorial.eu/01.basics/RadarPrinciple.en.html

[33] A. M. Hegazy and A. M. Hassan, "Fmcw software defined radar for range and speed estimation," *1st IUGRC International Undergraduate Research Conference Military Technical College, Cairo, Egypt*, July 2016. [Online]. Available: https://www.researchgate.net/publication/305737436

[34] M. A. Richards, *Fundamentals of radar signal processing.* McGraw-Hill Professional, 2005.

[35] M. I. J. Gamba., *Radar Signal Processing for Autonomous Driving*, 1st ed. Japan: Springer, 2020.

[36] L. Liang, H. Peng, G. Y. Li, and X. Shen, "Vehicular communications: A physical layer perspective," *IEEE Transactions on Vehicular Technology*, vol. 66, no. 12, pp. 10 647–10 659, 2017.

[37] M. Boban, A. Kousaridas, K. Manolakis, J. Eichinger, and W. Xu, "Connected roads of the future: Use cases, requirements, and design considerations for vehicle-to-everything communications," *IEEE Vehicular Technology Magazine*, vol. 13, no. 3, pp. 110–123, 2018.

[38] V. D. Khairnar and K. Kotecha, "Performance of vehicle-to-vehicle communication using ieee 802.11p in vehicular ad-hoc network environment," *International Journal of Network Security Its Applications*, vol. 5, no. 2, Mar 2013. [Online]. Available: http://dx.doi.org/10.5121/ijnsa.2013.5212

[39] W. Yuan, F. Liu, C. Masouros, J. Yuan, and D. W. K. Ng, "Joint radar-communication-based bayesian predictive beamforming for vehicular networks," 2020.

[40] C. Nguyen and J. Park , *Stepped-Frequency Radar Sensors Theory, Analysis and Design* . USA: Springer, 2016.

[41] L. Li and F. Wang, "Cooperative driving at blind crossings using intervehicle communication," *IEEE Transactions on Vehicular Technology*, vol. 55, no. 6, pp. 1712–1724, Nov 2006.

[42] Matlab, "Build a Driving Scenario and Generate Synthetic Detections," https://www.mathworks.com/help/driving/ug/build-a-driving-scenario-and-generate-synthetic-detections.html, 2020, [Online; accessed 25-May-2020].

[43] S. M. Patole, M. Torlak, D. Wang, and M. Ali, "Automotive radars: A review of signal processing techniques," *IEEE Signal Processing Magazine*, vol. 34, no. 2, pp. 22–35, 2017.

[44] F. Roos, J. Bechter, C. Knill, B. Schweizer, and C. Waldschmidt, "Radar sensors for autonomous driving: Modulation schemes and interference mitigation," *IEEE Microwave Magazine*, vol. 20, no. 9, pp. 58–72, 2019.

[45] M. U. Sheikh, J. Hämäläinen, G. David Gonzalez, R. Jäntti, and O. Gonsa, "Usability benefits and challenges in mmwave v2v communications: A case study," in *2019 International Conference on Wireless and Mobile Computing, Networking and Communications (WiMob)*, 2019, pp. 1–5.

[46] M. Boban, J. Barros, and O. K. Tonguz, "Geometry-based vehicle-to-vehicle channel modeling for large-scale simulation," *CoRR*, vol. abs/1305.0124, 2013. [Online]. Available: http://arxiv.org/abs/1305.0124

[47] C. Celes, F. A. Silva, A. Boukerche, R. M. d. C. Andrade, and A. A. F. Loureiro, "Improving vanet simulation with calibrated vehicular mobility traces," *IEEE Transactions on Mobile Computing*, vol. 16, no. 12, pp. 3376–3389, 2017.

[48] S. Uppoor, O. Trullols-Cruces, M. Fiore, and J. M. Barcelo-Ordinas, "Generation and analysis of a large-scale urban vehicular mobility dataset," *IEEE Transactions on Mobile Computing*, vol. 13, no. 5, pp. 1061–1075, 2014.

[49] W.-C. Lee and J. Krumm, "Trajectory preprocessing in computing with spatial trajectories," *Berlin, Germany: Springer*, pp. 3–33, 2011.

[50] G. Trajcevski, "Uncertainty in spatial trajectories," in computing with spatial trajectories," *Berlin, Germany: Springer*, pp. 63–107, 2011.

[51] J. H. H. W. H. Su, K. Zheng and X. Zhou, "Calibrating trajectory data for spatio-temporal similarity analysis," *The VLDB Journal*, vol. 24, p. 93–116, Feb. 2015.

[52] J. Khoury, R. Ramanathan, D. McCloskey, R. Smith, and T. Campbell, "RadarMAC: Mitigating radar interference in self-driving cars," in *2016 13th Annual IEEE International Conference on Sensing, Communication, and Networking (SECON)*, June 2016, pp. 1–9.

[53] WHO Media centre, "Electromagnetic fields and public health: radars and human health," https://www.who.int/peh-emf/publications/facts/fs226/en/#:~:text=The%20very%20low%20RF%20environmental,cause%20any%20significant%20temperature%20rise.&text=At%20present%2C%20there%

20is%20no,limits%20set%20by%20international%20standards., 2020, [Online; accessed 25-May-2020].